5-21-2017

Nonlinear Dynamics of Pulsing Oscillators

Christopher B. Fritz
Dickinson College

Nonlinear Dynamics of Pulsing Oscillators

Submitted in partial fulfillment of honors requirements
for the Department of Physics and Astronomy, Dickinson College,

by

Christopher B. Fritz

Advisor: Professor Lars Q. English

Reader: Professor Hans Pfister
Reader: Professor Robert Boyle
Reader: Professor Brett Pearson

Carlisle, PA
December 13, 2016

Abstract

Many oscillatory systems of great interest such as networks of fireflies, neurons, and relaxation oscillators exhibit pulsing behavior. The analysis of such oscillators has historically utilized a linear-phase model such as the Kuramoto equation to describe their dynamics. These models accurately describe the behavior of pulsing oscillators on larger timescales, but do not explicitly capture the pulsing nature of the system being analyzed. Indeed, the Kuramoto model and its derivatives abstract the pulsing dynamics and instead use a constantly advancing phase, thereby blurring the specific dynamics in order to fit to an analytically tractable framework. In this thesis, a modification is presented by introducing a phase-dependence to the frequency of such oscillators. Consequently, this modification induces clear pulsing behavior, and thus introduces new dynamics such as nonlinear phase progressions that more accurately reflect the nature of systems such as neurons, relaxation oscillators, and fireflies. The analysis of this system of equations is presented and the discovery of a heretofore unknown phenomenon termed ***periodic stability*** is described in which the phase-locked state of the system oscillates between stability and instability at a frequency determined by the mean phase. The implications of this periodic stability on the system such as oscillations in the coherence, or total degree of synchronization of the oscillator's trajectories, are discussed. The theoretical predictions made by this novel analysis are simulated numerically, and extended to real experimental systems such as electrical Wien-Bridge oscillators and neurons; systems previously described using the abstract Kuramoto model. Lattices constructed using this novel model yield predictions widely observed in real biological and chemical systems such as spiral waves. As a result, this model provides a fresh paradigm for exploring systems of coupled oscillators. The results of this work thus have clear implications on all real systems described presently by the Kuramoto model.

Acknowledgements

I want to thank all those family, friends, mentors, and colleagues whose past, present, and future support continues to carry me through even the heaviest of days. It is because of you this work is possible.

Contents

List of Figures

1 Introduction to Pulsing Oscillators: A Ubiquitous Problem in Nature and Machine

1.1 Neurons: A Biophysical Motivation for Understanding Pulsed Oscillations

There exists a large class of physical phenomena whose behavior may be described as series of periodic, discrete pulses. The pulse-like behavior of such a system is best described as when the majority of its time is spent in a constant, quiescent state, but nonetheless spends brief periods of time undergoing rapid change: pulses. The most clear way to illustrate this abstract definition is to turn to examples of pulsing systems.

Examples abound in both natural and man-made contrivances: the repeated flash of a firefly's bio-luminescent glow on a warm summer's night, the seemingly instantaneous leaps and precipitous drops in the voltage of a square wave, the life-giving beat of a pacemaker cell in the human heart, and the much dramatized beep it makes on a heart monitor. All of these systems exhibit what can most aptly be described as pulsing behavior.

The pulsing system presented for study here is the neural cell. In addition to being a fundamental building block of the nervous system, neural cells comprise the primary material present in human brains. These structures are of supreme interest in several disciplines of science for their biophysical properties; their role in representing, processing, and transmitting information; their crucial purpose in medical sciences (such as cardiovascular heart cells); as well as their functional position at the heart of modern artificial intelligence.

The analysis presented here will start from the ground up: explicit core assumptions will be made to model the physical behavior of the neuron. The purpose of this analysis is to uncover the pulse-like nature of the neuron explicitly from the differential equations governing its behavior, and to show the fundamental importance of understanding pulsing dynamics of such structures.

The entire work is organized as follows: Section 1 summarizes the current model for describing a system of neurons. It begins with the biophysics of a neuron, and expands to the abstraction of the Kuramoto method to systems of neurons. Section 2 introduces the new model and presents the full analysis of first the single-oscillator, then a set of coupled oscillators. It is in section 2 that the periodic stability is described as a result of a stability analysis. In section 3, the model predictions are compared to experimental data from real pulsing systems such as coupled Wien-

Bridge oscillators, and simulations of coupled neurons. Section 4 describes the explorations of populations of the novel model as a mechanism for understanding cognitive self-organization. Finally, section 5 discusses conclusions and suggestions for further research.

A note on numerical methods: Unless otherwise stated, all simulations implement a fixed-timestep 4^{th} order Runge-Kutta (RK4) method to calculate values. Specifically, Matlab's built-in *ode*45 solver was used. The timestep is configured such that the simulations produce accurate results and prevent error accumulation. In order to ensure accuracy, the time step is always configured as an order of magnitude below the threshold for error accumulation.

1.2 Physiological Considerations of a Neuron

This section seeks to understand how the pulsing behavior emerges from a neuron, as well as motivate the reader as to why studying neurons in particular is valuable. A neuron is a type of cell that is specialized to receive and transmit electrochemical signals to other cells in the body, often other neurons. Such signals are communicated via the release of chemicals called neurotransmitters. The crucial role neurotransmitters such as dopamine and serotonin play in behavior is highlighted by noting that modern pharmaceutical antidepressants are thought to work by modulating the concentration of these neurotransmitters [11]. Thus, understanding the dynamics of a neuron has deep implications for behavioral medicine.

Neurons consist of three primary components: the soma, a central body containing the cell nucleus; dendrites, which receive electrochemical input via synapses; and an axon which carries signals from the soma to a target cells via synapses [15]. Figure 1 displays a diagram of a typical nerve cell, where the soma consists of both the cell body and the nucleus.

Connections between one cell's axon and another's dendrite are referred to as synapses, which contain a small space called the synaptic cleft across which neurotransmitters flow during a neural firing. It is the synaptic connections that allow for many kinds of phenomena associated with networks of neurons such as learning and memory. Another common form of neural coupling is an electrical gap-junction, which is essentially a physical link between two synapses as opposed to a synaptic cleft. Synaptic plasticity, the changing of synaptic connection strength, is an important concept in computational neuroscience.

A neural cell's primary task is to communicate electrical signals referred to as action potentials, which typically occur when the soma's membrane potential, relative to fluid surrounding the cell, reaches a certain threshold voltage. When a neuron

Figure 1: A diagram of a typical neural cell. [1] Here the soma is labelled as the cell body. The myelin sheath occurs in many but not all neurons, and affects the speed at which electrical signals travel down the neuron's axon.

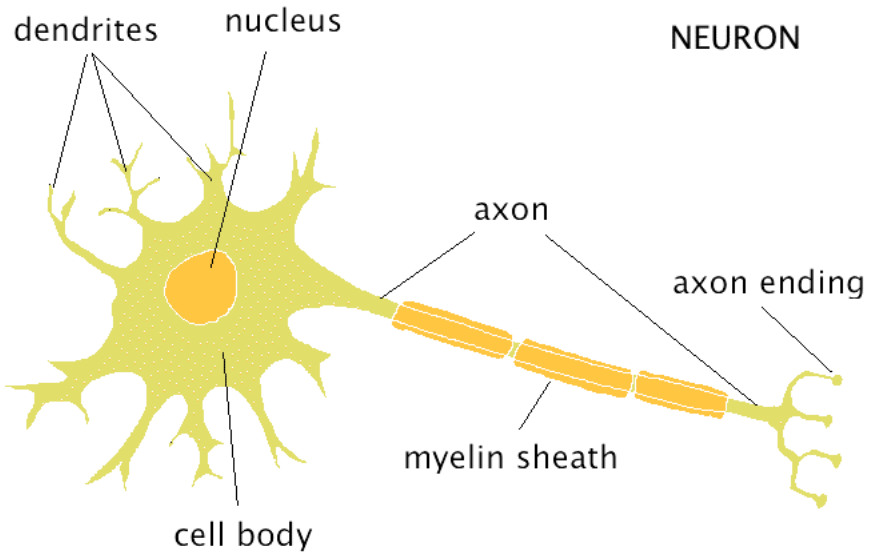

undergoes an action potential (also called a spike), neurotransmitters are released from its axons into the synaptic clefts and bind to receptors in the dendrites of the signal-receiving neurons. The reception of these neurotransmitters engenders a change in voltage in the neuron. If enough spikes are received and the neuron's voltage is sufficiently high, it will produce an action potential. In vitro neurons driven with currents in fact spike regularly producing so-called spike trains. [4]

Electrical potentials are produced by concentration gradients of ions such as K^+, Na^+, Cl^-, and Ca^{2+}. The equilibrium potential when no ions of species X are flowing across a membrane is given by the Nernst Potential [15]:

$$E_X = \frac{RT}{zF} ln \frac{[X_{outside}]}{[X_{inside}]} \tag{1}$$

where R is the universal gas constant, T is the temperature in K, z is the valence charge of the ion, and F is the Faraday constant. When a neuron generates a spike, the neuron's permeability to ions of a particular type changes. For example, at resting potential, the neuron may be very permeable to K^+, but when a spike occurs, the membrane becomes much more permeable to another ion, say Na^+ . This causes the membrane potential to rise, which sends the signal down the axon and causes the release of pre-synaptic neurotransmitters. If enough signals from various trans-

mitting (pre-synaptic) neurons are sent to a receiving (post-synaptic) neuron, it will generate a new action potential, thereby permeating the signal. These signals can travel relatively large distances, up to over 1 meter in an adult human in a time span of milliseconds [15].

Given that the information is represented electrically, neurons can be modeled mathematically as Resistor-Capacitor (RC) circuits, which can describe their electrical dynamics. Using Kirchhoffs Law, we write the total current flow, I, into a neuron as:

$$I = C\dot{V} + \sum_X I_X \tag{2}$$

where C is capacitance of the neuron (1.0 microFarads in a squid axon for example), V is the membrane voltage (the dot represents the time derivative), and X is the particular species of ion flow. One the left side of Eq. (2), the total current I is comprised of synaptic current, axial current, tangential current along the membrane surface, or current injected via an electrode. If none of these are present, then I is zero [8]. The individual ionic currents are proportional to the concentration gradient between the membrane potential and the species equilibrium potential given by the Nernst equation, and to the conductance of that ion across the membrane. For example:

$$I_K = g_K(V_{membrane} - E_K),$$

where g_K is the conductance of potassium across the membrane. Current flows through ion channels. While these channels are stochastic in nature, their probabilities are voltage-dependent. Therefore, sufficient current flow causes a channel to change its probability of usage. The channels are controlled by voltage-dependent gates of which there are two types: those that activate channels, and those that inactivate them. The probability of an activate-type gate being open is denoted by m (and n for different ion types). The probability of an inactivate-type gate being open is denoted by h. This occurs such that the total proportion of open channels is:

$$p = m^a h^b, \tag{3}$$

where a and b are the number of activation and deactivation gates, respectively.

The dynamics of the gating probabilities m and h are described by the differential equations

$$\dot{m} = \frac{m_\infty(V) - m}{\tau(V)} \tag{4}$$

and,

$$\dot{h} = \frac{h_\infty(V) - h}{\tau(V)}, \tag{5}$$

where m_∞ is the voltage-dependent activation-type gate probability the neuron would asymptotically reach if V were held constant, and is a voltage-dependent time constant [8]. The same definitions apply to the case of h. Both of the voltage-dependent functions are typically experimentally determined, but $m_\infty(V)$ and $\tau(V)$ are modeled as Boltzmann and Gaussian functions, respectively.

Assembling together our current understanding, we can generally describe the current flow due to a particular ion (Potassium in this case) through all the ion channels of a neuron as:

$$I_K = g_K m^a h^b (V - E_K). \tag{6}$$

It is worth noting that if a neuron has ion channels with only activation gates or only deactivation gates, then a or b is zero respectively, and the corresponding m or h term becomes 1, thus not affecting current flow.

One of the most widespread basic models of a neuron used in computational neuroscience, and the one which will be presented here, is the $I_{Na,p}+I_K$ model, usually referred to as "persistent sodium plus potassium" model. For more conductance-based models, see [8]. This particular implementation contains two ionic flow terms for Sodium and Potassium, as well as a leakage term (g_L), which considers the natural diffusion of ions across the membrane due to a potential gradient. The model is given by:

$$\begin{aligned} C\dot{V} &= I - g_L(V - E_L) - g_{Na} m(V - E_{Na}) - g_K h(V - E_K), \\ \dot{h} &= \frac{(h_\infty(V) - h)}{\tau(V)}, \\ \dot{m} &= \frac{(m_\infty(V) - m)}{\tau(V)}. \end{aligned}$$

Note firstly that we have rearranged our previous equation of current in favor of our dynamic variable of interest, voltage. Furthermore, in this model two primary types of ion flow occur, Potassium and Sodium. Finally, note that we have added an Ohmic leak term which is primarily due to Chlorine ion flow in through the membrane [8]. Experimentally, the Sodium type gating operates on a much faster timescale than the voltage change such that the system can be simplified without significantly obscuring the dynamics to:

$$\begin{aligned} C\dot{V} &= I - g_L(V - E_L) - g_{Na} m_\infty(V - E_{Na}) - g_K h(V - E_K), \\ \dot{h} &= \frac{(h_\infty(V) - h)}{\tau(V)}. \end{aligned} \tag{7}$$

Using parameters specified in the attached Matlab Code (See A.1), we can simulate the preceding equations for a neuron driven by a 10 pA input current.

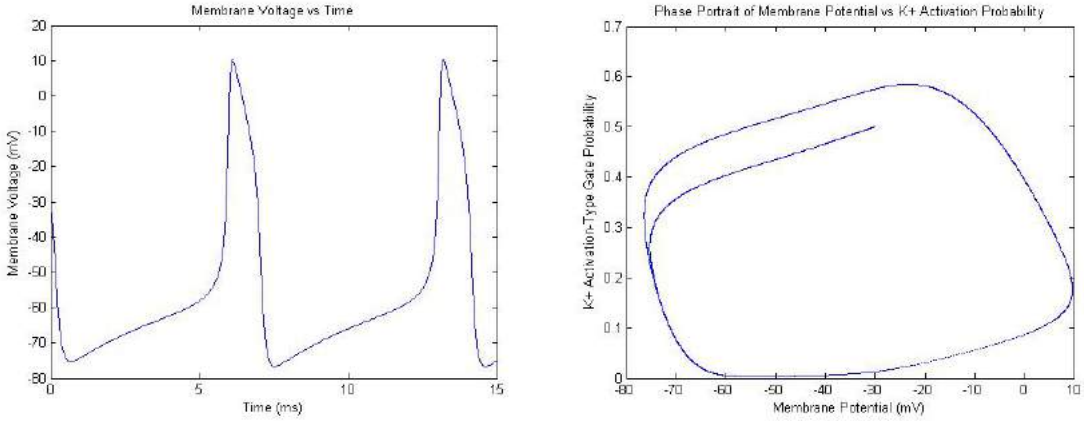

Figure 2: Left: A voltage versus time simulation of a single neuron driven by a 10pA current from the Persistent Sodium plus Potassium Model. Right: A Phase portrait of the membrane potential versus K^+ gate activation probability. Note that the trajectory quickly settles on a stable limit cycle. The limit cycle bifurcates from a stable node as input current, I increases from 0.

Methods from dynamical systems have been applied to such models to analyze the different types of behavior a neuron can exhibit. For example, in Fig. 2, the behavior of the membrane potential is a constant spike train, and the phase plane consisting of membrane potential and K^+ activation probability shows that the system has settled into a stable limit cycle. This limit cycle is created via an Andronov-Hopf bifurcation as the net current, I, is increased from zero [8]. Such a bifurcation is described as when a system parameter (in this case I) changes such that the system changes drastically from a steady state (i.e constant membrane potential) to periodic behavior of some sort (i.e periodic pulses). The bifurcation creates a limit cycle in the phase space between membrane voltage and activation probability of the K channel. No current input to the neuron would consequently be represented as a straight line in the left pane of Fig. 2 corresponding to a steady membrane potential in time. The right panel would only display a single point representing the state of the neuron if no current were injected.

As described before, two neurons communicate information through various forms of synapses. It is thus necessary to alter our dynamical model to account for the presence of other neurons. We will assume they are coupled via electrical gap-junctions for simplicity. Gap junctions allow ions to flow directly between neurons, at a rate

proportional to the potential gradient between the two neurons. Thus for a particular neuron, $j = 1, 2, ...N$, that is physiologically (in terms of parameters) identical to N other neurons our new model is:

$$\begin{aligned} C\dot{V_j} &= I_j - g_L(V_j - E_L) - g_{Na}m_\infty(V_j - E_{Na}) - g_K h(V_j - E_K) + \frac{K}{N}\sum_{i=1}^{N}(V_j - V_i), \\ \dot{h_j} &= \frac{h_\infty(V_j) - h_j}{\tau(V_j)}. \end{aligned} \tag{8}$$

Note that the K in the summation term refers to coupling strength between neurons, whereas the K in the immediately preceding term represents the Potassium ion species flow. This ambiguity is due to convention which represents coupling strength by the letter K, as will be done for the remainder of this thesis.

Figure 3: Coupled Driven Neurons for various Values of Coupling Strength, K. Left: K = 0, the undriven neuron is at steady equilibrium potential. Right: K = .01, the weak coupling causes the undriven neuron to spike, but at a phase lag and slightly altered waveform compared to the driven neuron. Bottom: K = .5, the strong coupling locks the two neurons in phase and precisely synchronizes them. (I = 20 pA).

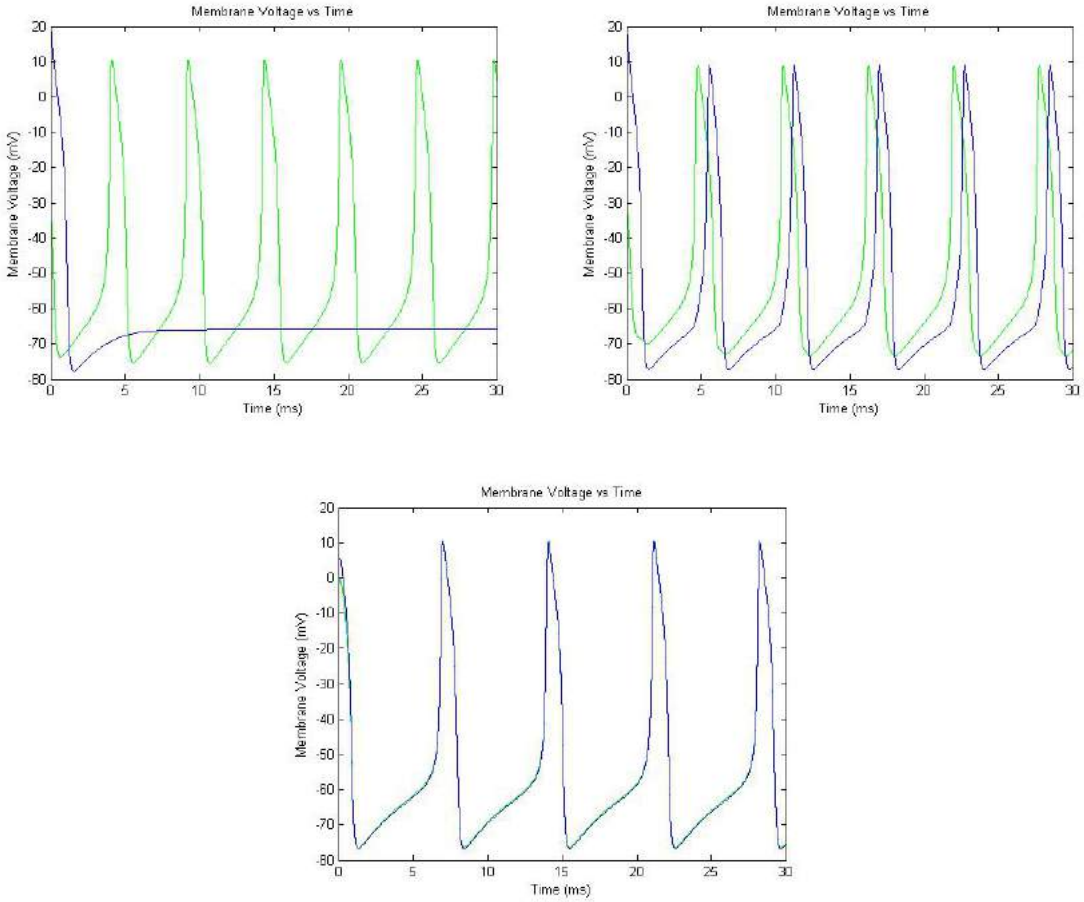

Figure 3 displays the behavior of two neurons connected as the coupling strength between them is varied. One is driven with constant current I, the other driven only by the connection via coupling. We see that the coupling strength radically alters the behavior of the driven neuron, and that for sufficient coupling strengths, perfect synchronization occurs. It is important to note, however, that our driving current is a constant value, whereas the input current in a real pair of coupled neurons is subject to noise such that the firings are stochastic [4]. This method of simulation is computationally complex and not mathematically convenient for analysis. Thus it is necessary to reduce our model further to more deeply understand the dynamics of a population of such oscillators.

1.3 The Limit Cycle Approximation & Kuramoto's Model

This section details the analysis of systems of neurons using the Kuramoto model abstraction. The existence of a limit cycle immediately implies periodic behavior of some sort for a neuron. As such, it is possible (and mathematically convenient) to model a neuron as a phase oscillator. A phase oscillator is described as a periodic sinusoidal signal which has some phase which is a function of time. We only consider the case in which the neuron is firing and a limit cycle exists, given that a steady equilibrium state should not be considered an oscillator. A limit cycle occurs when a closed trajectory is created in the phase-space of a system. For example, if the position of an object is described by a sine term, then the velocity is a cosine term. The phase space of this system is its position vs. its velocity, and thus is a circle in the case of a simple harmonic oscillator. In this context, it makes sense to define a phase variable, ϕ, which describes the location of the neuron along the limit cycle. Naturally, the neuron's phase space is not identical to a harmonic oscillator, hence the abstraction. When the phase reaches a certain value, say maximum membrane potential, the neuron is said to have fired, thus we reset the phase to zero. With this treatment in Fig. 2a, the driven neuron undergoes one complete oscillation from the peak around approximately every 8 milliseconds. If the neuron does not immediately start on the limit cycle, its trajectory will asymptotically approach the limit cycle, and we can treat the system identically to the case where it begins on the limit cycle.

There are numerous topological arrangements (i.e ways in which things are connected to one another) of coupled oscillators that can be considered. Modelling synaptic plasticity, the basis of learning, involves dynamically altering the coupling between two such oscillators [4](chapt. 8). The Kuramoto model, which treats arrays of globally coupled oscillators, is widely used to study neural systems and synchronization [12].

Here we consider the case of globally coupled neurons, meaning each neuron will be connected to each other via synapse. An important model of globally coupled, limit-cycle oscillators is the Kuramoto model:

$$\dot{\phi}_i = \omega_i + \frac{K}{N}\sum_{j=1}^{N}\sin(\phi_j - \phi_i) \tag{9}$$

where ϕ_i is the phase of oscillator i, ω_i is the natural frequency of oscillator i, K is the coupling strength, and N is the number of oscillators. In the Kuramoto model, each oscillators frequency is shifted by every other oscillator in the network by an amount proportional to the global coupling strength K, and the sine of their phase difference. Kuramoto systems are capable of global synchronization. By synchronization, we

mean the capacity for each oscillator to become phase-locked despite the difference in natural frequency and initial condition. We measure the level of synchrony by defining an order parameter, r, such that

$$re^{i\psi} = \frac{1}{N}\sum_{j=1}^{N} e^{i\phi_j(t)}, \tag{10}$$

where r is the order parameter and ψ is the mean phase. Note that,

$$|r^2| = \frac{1}{N^2}\left[\Big(\sum_j \cos\phi_j\Big)^2 + \Big(\sum_j \sin\phi_j\Big)^2\right], \tag{11}$$

which is the parameter best used to measure synchrony. The order parameter is a convenient macroscopic quantity that provides information about the state (namely phase and synchrony level) of every oscillator in the network.

Correspondingly, the mean phase ψ can be calculated numerically as:

$$\sin(\psi(t)) = \frac{1}{r(t)N}\sum_{j=1}^{N} \sin\Big(\phi_j(t)\Big), \tag{12}$$

Using the order parameter, r, it can be shown [16] that the Kuramoto model reduces to the mean-field model given by

$$\dot{\phi}_i = \omega_i - Kr\sin(\theta_i)$$

where $\theta_i = \phi_i - \psi$ is the drift phase of the oscillator from the mean phase of the network. See section 2 for a derivation of this identity. Thus each oscillator's phase only depends on its difference from the average phase of every oscillator in the system. The mean-field model significantly simplifies the system such that it becomes much more mathematically tractable. The question we now ask is how does synchrony depend on the coupling, K? The critical coupling which induces synchronization depends on the distribution of frequencies of the oscillators, Ω. In simulations, ω_i is typically determined by a random number generator with a Gaussian probability distribution. The threshold value of coupling for which synchronization occurs can be formally derived as a function of the standard deviation of the frequency distribution of each oscillator:

$$K_c = \sigma\sqrt{\frac{\pi}{8}}$$

where σ is the standard deviation of the frequency distribution. This equation implies that the larger spread in the natural frequencies of the oscillators (the more different they are), the higher coupling strength will be required to even partially synchronize them.

Figure 4: Oscillator Phases and Corresponding Order parameter graphs. Each graph gives the real time calculation of the order parameter during a simulation demonstrating spontaneous synchronization. Top Left: The system's phases are distributed evenly at the beginning of the simulation, corresponding to a low order parameter. Top Right: The System begins to cluster with a portion of oscillators still distributed evenly. The order parameter increases correspondingly. Bottom: The system has synchronized nearly and all oscillators are phase-locked, save a few drifting near the cluster. As such, the order parameter has nearly reached its maximum value. (It asymptotically approaches 1).

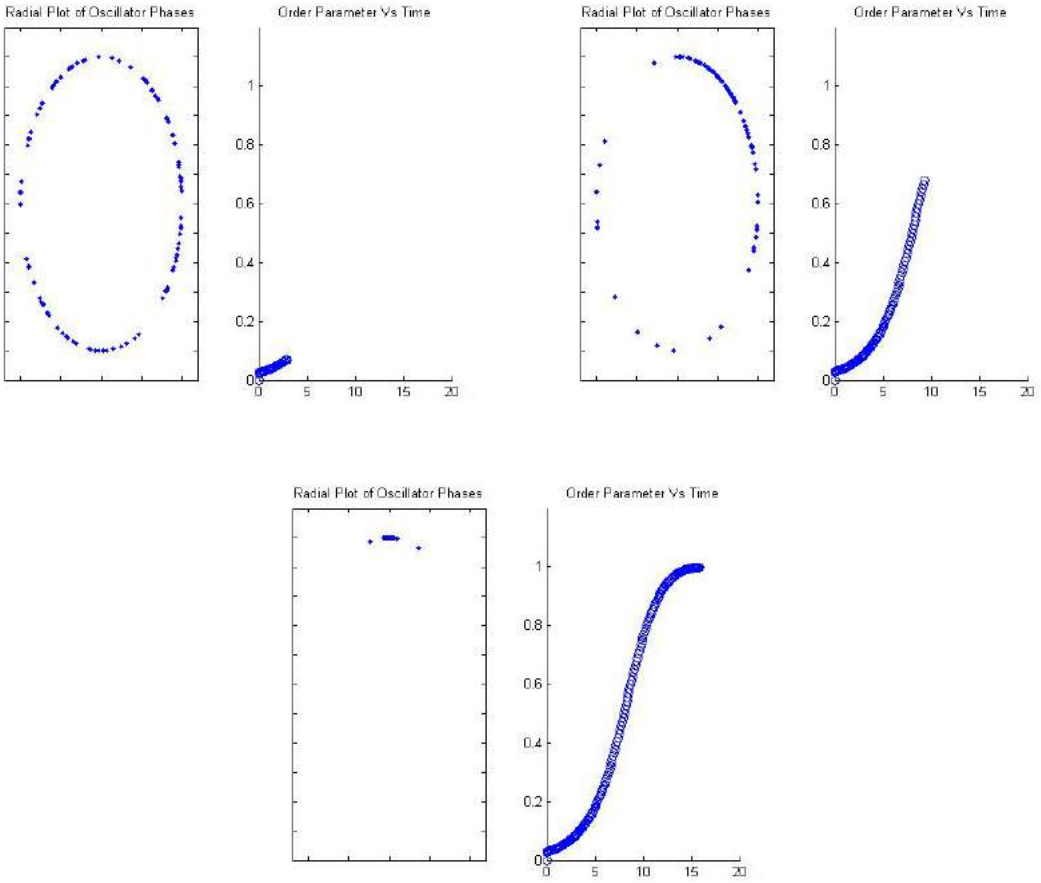

We see that the system is capable of global synchronization in which each oscillator locks phase. The left series of figures in Fig. 4 can be interpreted as the position of each neuron along the limit-cycle in the phase plane as in Fig. 2. The right series of figures give the associated order parameter. As expected, as the phases come closer together, the order parameter increases until reaching a maximum at just below 1. Synchronization phenomena such as this are widespread in neural systems.

Partial synchrony may be responsible for the production of brain oscillations such as alpha and gamma waves and EEG rhythms. Specific patterns of coordinated firing of neurons is a characteristic of pathological activities such as epilepsy. As such, the bridge we have spanned, from the physics of a single neuron to the global synchronization of an arbitrary number of neurons provides an introduction to the understanding of neuroscience through nonlinear dynamical systems.

We have thus summarized a relevant portion of the current knowledge of neurons viewed as pulsing oscillators. In the next section, we proceed to introduce a novel modification to the Kuramoto model as a high-order model for pulsing oscillators.

2 Active Rotators: A Better Model for Pulsing Oscillators

Before continuing with the new model, it is first necessary to discuss the limitations of the Kuramoto model in describing the behavior of a pulsed oscillator.

The primary limitation of Eq. 9 lies in the constant natural frequency which is only slightly modulated by coupling. Once synchronized, the phase oscillator proceeds linearly at the mean frequency. This model is valid when the oscillator it describes has a similar linearly increasing phase. However, for the case of pulsing oscillators such as the neuron, this is inaccurate. The typical solution to this problem has been to represent the phase as an abstract value separate from the actual functional waveform of such oscillator. In other words, as the phase passes through some value such as $2\pi n$, the oscillator is said to have pulsed. As such this method captures only the periodic nature of such pulsing oscillations, and eschews any functional approximation of a pulse. That is, a pulsing oscillator is abstracted as functionally identical to a continuous phase sinusoidal oscillator. Because this model is used to study populations of oscillators, the pulsing nature of a single oscillator has no impact on the predicted dynamics of interacting populations.

Here, a different model of oscillator is presented. A phase-dependent term is inserted into the natural frequency of the oscillator such that the oscillator travels quickly through certain value of phase, while it travels especially slowly through others. The net effect is that the oscillator will undergo rapid changes over short periods of time while the majority of its time will be spent in a quiescent state. Our model for a single uncoupled oscillator is thus:

$$\dot{\phi} = \omega(1 + b\sin\phi), \tag{13}$$

where b is strictly between 0 and 1. This is essentially the active rotator model

detailed by Shinomoto and Kuramoto in their work in the late 1980's, with some slight modifications. [9]

2.1 Analysis of a Single Uncoupled Oscillator

Equation (13) can be solved explicitly, but first it is useful to discuss the behavior qualitatively. Assuming $\phi(0) = 0$, then the oscillator will proceed with an increasing velocity until it reaches a maximum velocity of $\dot{\phi} = \omega(1+b)$ at $\phi = \frac{\pi}{2}$. The symmetry of the sine function means that the phase velocity will slow down in exactly the same manner as it sped up. It will thus rapidly decrease its velocity until it reaches the minimum velocity of $\dot{\phi} = \omega(1-b)$ at $\phi = \frac{3\pi}{2}$. It is clear here that as $b \to 1$, the oscillator will slow down further toward $\dot{\phi} = 0$. For $b = 1$ a fixed point exists at $\phi = \frac{3\pi}{2}$. This model thus takes advantage of the ghosting effect, which is an intense slowing down of the phase velocity near the bifurcation point b=1.; as b approaches the fixed point value, the oscillator spends more and more time stuck in this bottleneck around the fixed point $\phi = \frac{3\pi}{2}$. Combining the effects of both the rapid increase and rapid decrease in velocity, along with near-stoppage of the oscillator from the ghosting effect, we have thus created a qualitative picture of the oscillator's behavior over a single cycle.

To integrate equation (13), we first use separation of variables:

$$\frac{d\phi}{1 + b\sin\phi} = \omega dt.$$

Integrating the right side is trivial, but the left side appears deceptively simple. In fact it is much more involved. Using a computer algorithm [18] to solve this integral yielded the following:

$$\frac{2tan^{-1}\frac{b+tan\frac{\phi}{2}}{\sqrt{1-b^2}}}{\sqrt{1-b^2}} + constant = \omega t. \tag{14}$$

Equation (14) is a useful form as we will see shortly. For now, we solve Eq. (14) for ϕ to finally obtain an expression for phase:

$$\phi = 2\tan^{-1}\left[\sqrt{1-b^2}\tan\left((\omega t - C)\frac{\sqrt{1-b^2}}{2}\right) - b\right], \tag{15}$$

where C is the constant of integration. The only note is that the tangent term in this solution is π periodic, whereas the phase variable ϕ is 2π periodic. Therefore it is necessary to graft discontinuities as ϕ reaches multiples of π so that the solution to a single oscillator is monotonic (always increasing). Matlab's *unwrap()* function accomplishes this exactly.

With this solution in hand, we now examine how varying the parameter b alters the trajectory of the solution. Figure 5 shows the traces of several trajectories each with a different value of b. The initial condition for each trajectory was $\frac{3\pi}{2}$.

Figure 5: Top: Phase vs. Time of a single uncoupled oscillator for various values of b. The phase was unwrapped such that it is continuously increasing and not modulo 2π. The natural frequency, ω of the oscillator was 2π, and b is measured as a percentage of ω. Bottom: The sine of the phase illustrates pulsing nature of the oscillation for $b = .99$. The vertical lines in both instances represent the calculated pulse times according to equation 16 for the case that $b = .99$ and $\omega = 2\pi$.

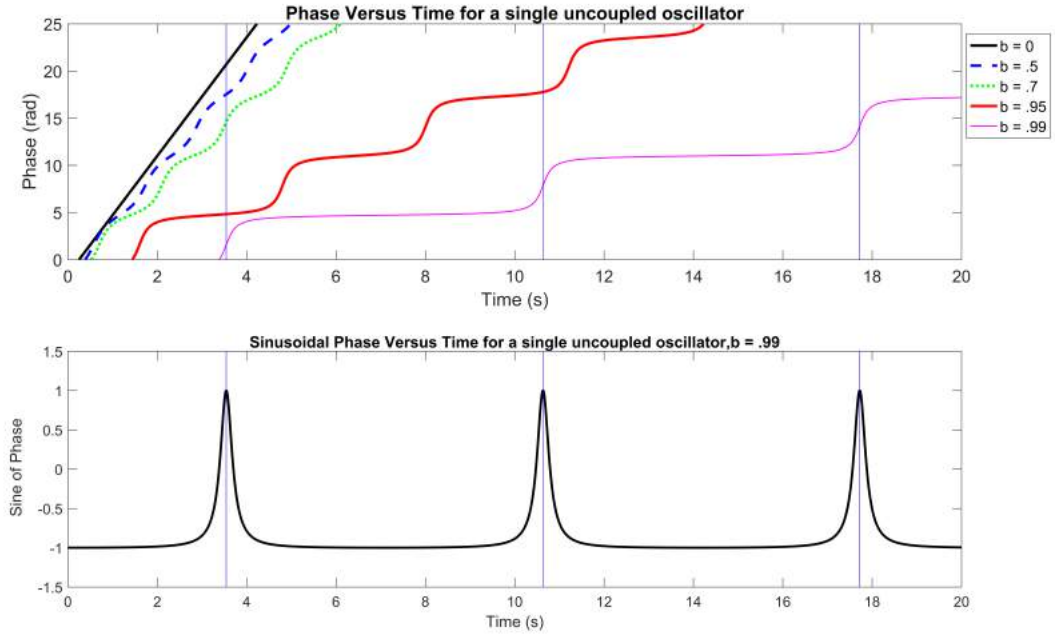

The two most striking features of these traces are the stair-case progression of phase and the strong resemblance to a series of Dirac delta spikes that the sine of the phase exhibits. In this way the pulsing of the oscillator is clearly visible. Functionally, our oscillator behaves just as a real system that pulses in a continuous manner. We no longer abstract the phase to continuous motion while the oscillator is resting. When the oscillator does not pulse, the phase essentially stops and only resumes during another pulse. This effect becomes more extreme as $b \to 1$.

In theoretical neuroscience, neuronal firings are characterized by a discrete series of pulse times. The general consensus is that the timing of pulses is where the information is stored [4]. Thus it is useful for our model to produce an equation for

the associated pulse times of a single oscillator. This is accomplished using Eq. (14). By setting $\phi = \frac{\pi}{2}$ and solving for t we can calculate the time it takes for the trajectory to reach its first pulse:

$$t^0_{pulse} = \frac{2}{\omega\sqrt{1-b^2}} \tan^{-1}\left(\frac{1+b}{\sqrt{1-b^2}}\right) + \frac{C}{\omega}.$$

The next pulse occurs when the inverse tangent term has proceeded to π twice, and thus the k^{th} pulse occurs at a time:

$$t^k_{pulse} = \frac{2}{\omega\sqrt{1-b^2}}\left[\tan^{-1}\left(\frac{1+b}{\sqrt{1-b^2}}\right) + k\pi\right] + \frac{C}{\omega} \tag{16}$$

The resulting pulse times are evenly spaced, therefore we can calculate the frequency by subtracting $t_{k+1} - t_k$ which yields:

$$\omega_{pulse} = \omega\sqrt{1-b^2}.$$

This equation resembles the Lorenz contraction that occurs due to relativistic (appreciably near the speed of light) velocities of matter. The frequency thus represents an interesting parallel between our system and temporal-spacial deformation high-velocity material objects. Although this connection appears superfluous, and is merely a curiously similar expression.

2.2 Analysis of Multiple Coupled Oscillators: Discovery of Periodic Stability

Having a basic understanding of the dynamics of a single oscillator, we now proceed to analyze a system of globally coupled oscillators. Similar to Eq. (9), we assume a sinusoidal coupling scheme such that our system is described by:

$$\dot{\phi_i} = \omega_i(1 + bsin\phi_i) + \frac{K}{N}\sum_{j=1}^{N}\sin(\phi_j - \phi_i) \tag{17}$$

For the purposes of analysis, it is convenient to represent this system in mean field form. That is, each oscillator is not viewed as globally coupled to every other oscillator in the network. Rather, a macroscopic mean-field, which is essentially the average, is connected to each individual oscillator. In this way, oscillators are effectively decoupled from one another, and instead to a single uniform driver. Analytically, this simplifies the calculation greatly. Note that if we multiply both sides of Eq. (10) by $e^{-\phi_i}$, then we obtain

$$re^{(i\psi-\phi_i)} = \frac{1}{N}\sum_{j=1}^{N} e^{i(\phi_j-\phi_i)}$$

Taking the imaginary components of both sides here,

$$r\sin(\psi - \phi_i) = \frac{1}{N}\sum_{j=1}^{N}\sin(\phi_j - \phi_i),$$

and substituting this into our model, Eq. (17), thus yields

$$\dot{\phi_i} = \omega_i(1 + b\sin\phi_i) + Kr\sin(\psi - \phi_i). \tag{18}$$

In this form, we represent each oscillator as being driven by its own spatially-modulated intrinsic frequency, and also being pulled towards the rest of the cluster by a force dependent on the coupling strength and the synchrony of the system. Notice here how we have isolated each oscillator i from every other j^{th} oscillator. Furthermore, we need no longer deal with a sum inside the differential equation. These are the two reasons the mean-field form is advantageous.

Using the approach as outlined by Strogatz [17], the first step to analyzing such a system is to fix the frame at the mean phase, ψ. Before we can do this, however, we must first explicitly characterize ψ. We begin with the simplest case that each oscillator is identical and starts at some random phase and observe the behavior of the system.

Figure 6: Spontaneous Phase-locking of 100 coupled oscillators with identical frequencies. The coherence is calculated using Eq. (11). The time step for this simulation was a tenth-milisecond. The natural frequency of each oscillator is 8π, and the phases are initialized in a Gaussian distribution about $\frac{3\pi}{2}$ with a standard deviation of 1; K =1.

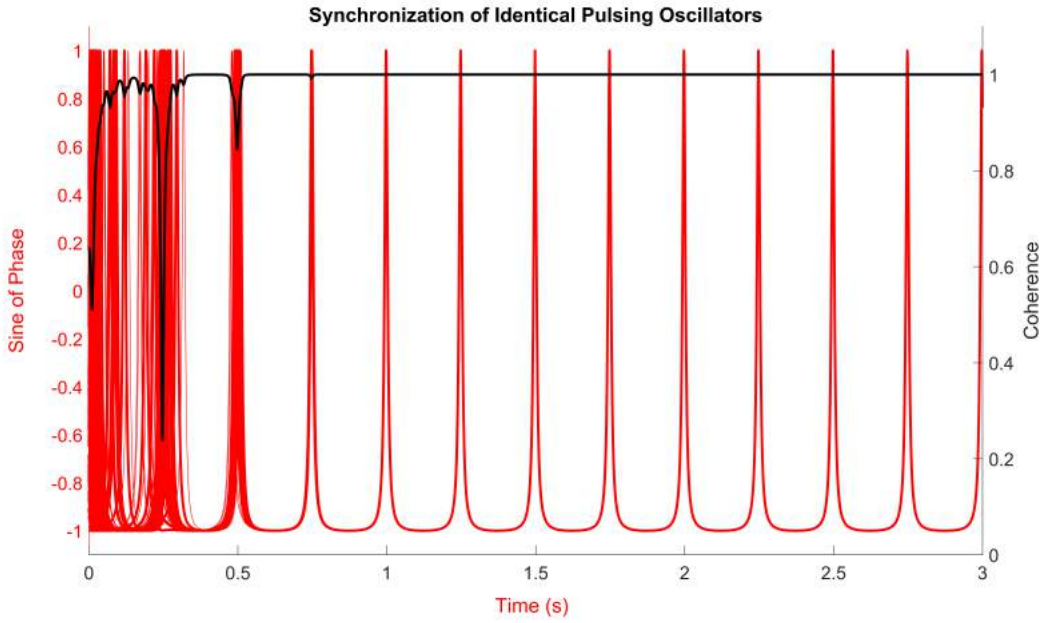

From Fig. 6 we can see very clearly that the oscillators quickly converge from 100 individual trajectory into one indistinguishable solution, where each oscillator pulses in unison. This is only the case for identical-frequency oscillators, but the analysis of this case will yield useful results which apply to the case of a distribution of frequencies as well. In this phase-locked case, it is clear that the trajectory of the mean phase, ψ, can be described as that of a single oscillator solution. Therefore we are justified with the statement that

$$\dot{\psi} = \Omega(1 + b\sin\psi). \tag{19}$$

Now that we have sufficiently characterized the mean phase, we attempt to transform the system into the rotating frame specified by:

$$\theta_i(t) = \phi_i(t) - \psi(t),$$

and consequently:

$$\dot{\theta}_i = \dot{\phi}_i - \dot{\psi}.$$

Our transformed system is described by:

$$\dot{\theta}_i = \omega_i\big[1 + b\sin(\theta_i + \psi)\big] - Kr\sin\theta_i - \Omega\big(1 + b\sin\psi\big).$$

The presence of the modulation term ensures that even the expression for $\dot{\theta}_i$ will still contain ψ, thus our transformation does explicitly eliminate the mean phase. This is the principal cause of difficulty in the analysis of this system. Previous analysis of the globally-coupled system utilized a mean-field model that treated every oscillator as individually coupled to some mean field. By rotating the frame at this mean field, each oscillator could thus be isolated completely and its drift described in terms of its intrinsic frequency relative to the mean frequency of the distribution of oscillators. [17]. However, our spatial modification requires that we must know the mean phase at all times to properly describe the dynamics of a particular oscillator, and that the behavior of any deviations of the oscillator from the cluster are specific to the particular point through which the mean phase is passing. Thus we cannot simply rotate out the mean phase. To analyze this system, therefore, we will use tools from nonlinear analysis.

For synchronization to occur, the frequencies must be reasonably close to one another. This imposes a limit on the magnitude of deviation of each oscillator from the mean frequency of the system. As such, $\omega_i - \Omega$ must be sufficiently small. In this thesis, we assume that the standard deviation of these frequencies about the mean, σ, is less than 10% of the mean frequency. (I.e $\sigma \leq .1\Omega$)Since ω_i is a small deviation η_i from Ω, the average frequency, we substitute $\omega_i = \Omega + \eta_i$ to obtain:

$$\frac{d\theta_i}{dt} = [\Omega + \eta_i]\big[1 + b\sin(\theta_i + \psi)\big] - Kr\sin\theta_i - \Omega[1 + b\sin\psi] \tag{20}$$

where $|\eta| << 1$.

Recall that we are first considering the case where $\eta_i = 0$ for all oscillator; all frequencies are identical. In this case, as θ_i passes through 0 it reaches a fixed point. To see this, simply substitute $\theta_i = 0$. Note here that no assumptions were made for ψ. Indeed 0 is a fixed point regardless of the value of ψ. At this fixed point, the cluster will be perfectly synchronized for all time because θ_i is necessarily 0 for all oscillators. Since θ_i is the deviation from the mean phase of the i^{th} oscillator, this implies all oscillators are perfectly fixed to the mean phase, ψ. Therefore it is necessarily true that $\phi = \psi$.

To analyze the stability of this fixed point we utilize a linear approximation of the system. This linearization produces analytically tractable terms that can yield useful

predictions for an otherwise opaque system's dynamics. We are concerned with the behavior of an arbitrary oscillator. The mean field approach allows us to describe a single oscillator as it interacts with the mean field only. Given that the fixed point exists (i.e $\theta_i = 0$ independent of ψ), we can extend our analysis here generally to every oscillator in the globally coupled system.

The stability analysis uses a linear approximation which is analogous to a Taylor series. The stability of a solution determines how much a small perturbation will grow in time. If it is unstable the solution will expand exponentially from the fixed point, whereas a stable point will be impervious to small perturbations and the trajectory will remain at the fixed point. With this in mind, the stability at $\theta_i = 0$ for the system described by Eq. (20) is given by

$$\frac{\partial \dot{\theta}_i}{\partial \theta_i} = \big[\Omega + \eta_i\big] b \cos(\theta_i + \psi) - Kr \cos\theta_i \tag{21}$$

Again allowing the previous assumptions that $\eta_i = 0$, and that θ_i is at its fixed point 0, Eq. (21) reduces to:

$$\Omega b \cos\psi - Kr \tag{22}$$

We define λ such that

$$\lambda \equiv \Omega b \cos\psi - Kr \tag{23}$$

Essentially this tells us how perturbations grow in time, whether they decay toward the fixed point, or grow exponentially at a speed governed by λ and in a direction governed by the eigenvector. As such, we can approximate the behavior of solutions near the fixed point $\theta_i = 0$. In this case a perturbation from the fixed point of the i^{th} oscillator, δ_i grows as,

$$\theta_i = \delta_i e^{i\lambda}. \tag{24}$$

The sign of λ thus determines the stability of the solution. But Eq. (23) shows that λ is not always positive or always negative. In fact, λ is periodic in ψ, which continually advances. Therefore, the stability of the fixed point $\theta_i = 0$ is periodic. Furthermore, this term explicitly depends on K, Ω, b, and r. This applies to every oscillator in the system, thus the entire system exhibits this *periodic stability*. This phenomenon has not, to the author's present knowledge, been explicitly described in nonlinear dynamics literature, although its signs have been described by Shinomoto and Kuramoto [9]. Notably, they observed oscillations in the number density of a system of these rotators. The number density is analogous, although not identical, to the coherence of the system.

Before we stated that all trajectories on the fixed point stay there for all time. This statement is still correct. But the existence of the current fixed point relies

on all trajectories being at the same phase and having the same intrinsic frequency. Real systems rarely have exactly identical properties and are subject to noise. As a result, solutions are constantly perturbed by noise terms. To model this, we introduce Gaussian white noise with a flat frequency spectrum, so that the signal to noise ratio is 70 dB.

Figure 7: Coherence vs. time of 250 coupled oscillators driven with Gaussian white noise. The coherence is calculated using equation 11. At each time step, the phases were driven with a flat-frequency-spectrum noise signal such that the signal to noise ratio was 70dB. The simulation is colored according to the value of λ_2 as calculated by equation 23, which is then normalized. The time step for this simulation was a tenth-milisecond. The natural frequency of each oscillator is 8π, and the phases are all initialized at $\phi_o = 0$; K =1.

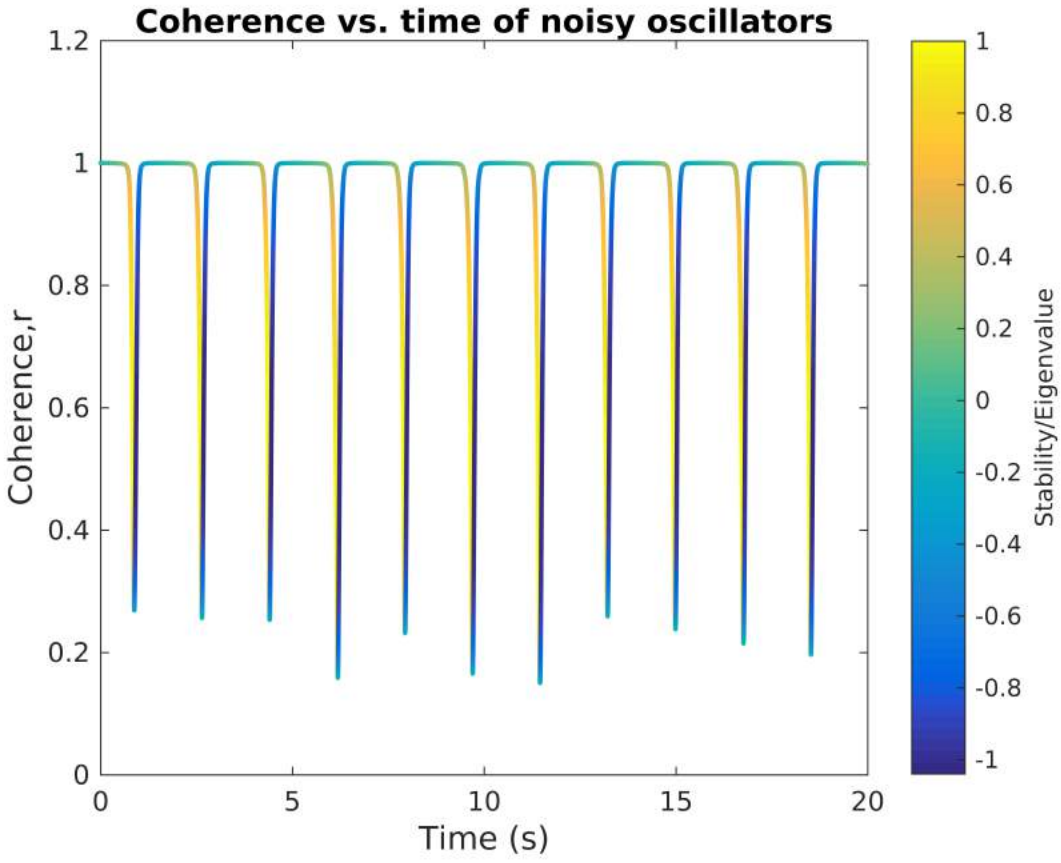

Figure 7 shows the coherence of the system with the color of the trace specified by the value of λ as calculated by Eq. (23). We can clearly see that the stability determines whether or not the coherence of the system drops. For positive stability (yellow), the fixed point becomes unstable, and the noise grows exponentially, causing

the phases to spread out and dropping the coherence of the system. As ψ continues, however, the stability approaches zero (green) and symmetrically decreases to negative one (blue). This causes the phases to re-synchronize as the stability causes the noise to decay exponentially.

Although we have only considered the case where $\eta_i = 0$ thus far, it is not difficult to extend our results to a distribution of frequencies. Instead of using a Gaussian white noise to drive the solutions, we interpret the frequency distributions as providing a constant noise to the system. To show this, consider the stability in θ_i about the fixed point with a nonzero η_i which is given by

$$\frac{\partial \dot{\theta}_i}{\partial \theta_i}_{\theta_i=0} = \big[\Omega + \eta_i\big] b\cos(\psi) - Kr$$

Averaging both sides of the previous equation over all oscillators i yields:

$$\begin{aligned}
\left\langle \frac{\partial \dot{\theta}_i}{\partial \theta_i}_{\theta_i=0} \right\rangle_i &= \Big\langle \big[\Omega + \eta_i\big] b\cos(\psi) - Kr \Big\rangle_i \\
&= \Big\langle \eta_i b\cos(\psi) + \Omega b\cos(\psi) - Kr \Big\rangle_i \\
&= \Big\langle \eta_i b\cos(\psi) \Big\rangle_i + \Omega b\cos(\psi) - Kr \\
&= \Omega b\cos(\psi) - Kr = \lambda,
\end{aligned} \tag{25}$$

where the last equality follows because η_i is a Gaussian distribution about 0. To see this, note that:

$$\omega_i = \Omega + \eta_i,$$

$$\Rightarrow \big\langle \omega_i \big\rangle_i = \big\langle \Omega + \eta_i \big\rangle_i,$$

$$\Rightarrow \big\langle \omega_i \big\rangle_i = \Omega + \big\langle \eta_i \big\rangle_i$$

$$\Rightarrow \Omega = \Omega + \big\langle \eta_i \big\rangle_i$$

$$\Rightarrow \big\langle \eta_i \big\rangle_i = 0.$$

Equation (25) immediately implies that the distance θ_i grows from the fixed point $\theta_i = 0$, is governed by λ as calculated before in Eq. (23). Thus a frequency distribution of oscillators should also display this periodic stability. In this way the mean field approach can tell us at what points the system will synchronize or lose coherence. So we see once again the periodic stability exhibited by the system. However, because

the intrinsic natural frequencies do not change, the noise from their distribution is constant, thus the same drop in coherence is observed for each oscillation, whereas before in figure 7, the coherence dropped randomly as the system was driven by noise.

Figure 8: Coherence, stability vs. time of 250 coupled oscillators. The coherence is calculated using equation 11. Each oscillator has a frequency which is distributed about $\Omega = 8\pi$ using a standard deviation of $.05\omega$. The simulation is colored according to the value of λ as calculated by equation 23, which is then normalized. The time step for this simulation was a tenth-milisecond. The natural frequency of each oscillator is 8π, and the phases are initialized at $\frac{3\pi}{2}$; $K = 1$.

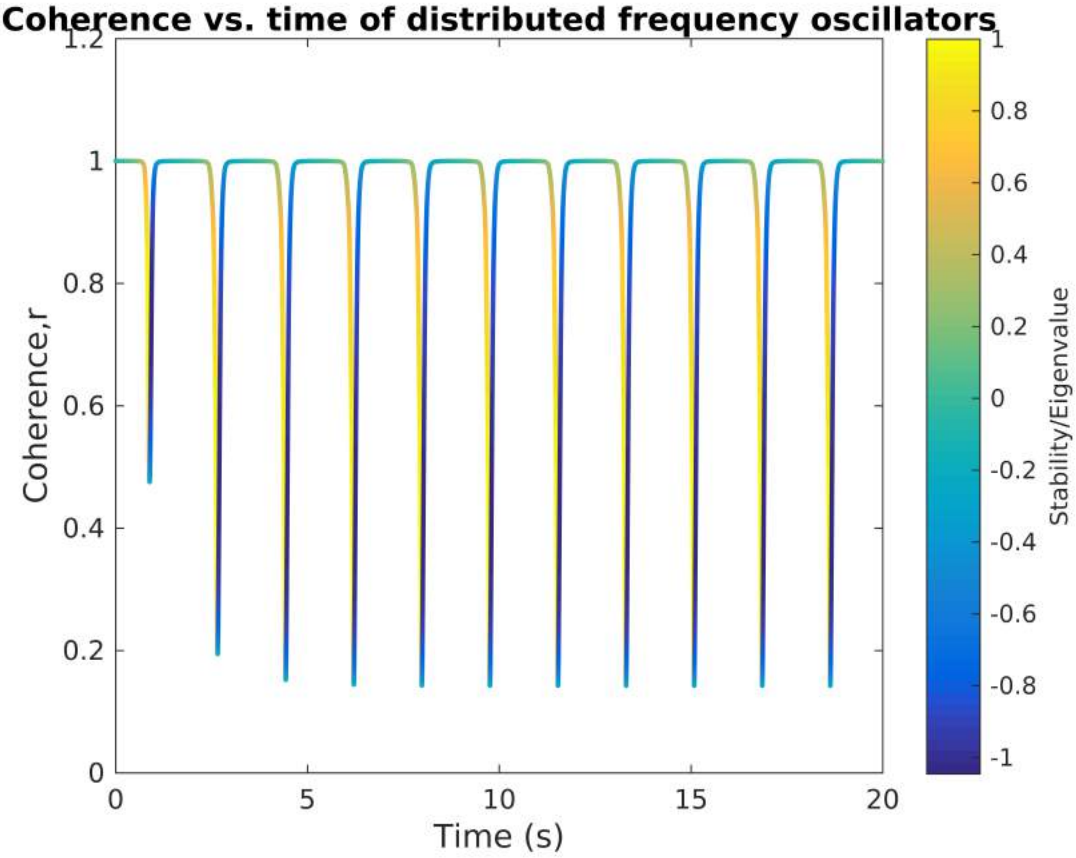

Equation (23) suggests a new regime for coupling. Namely, that the coupling strength K is on the order of Ωb as it influences the synchronized stability. Therefore we define a new coupling strength $\tilde{K} = \frac{K}{\Omega b}$. Given that Fig. 7 used a value of $K = 1$, this corresponds to a coupling strength of $\tilde{K} = \frac{1}{8\pi.99}$. Exploring the effect of varying coupling strength, $\tilde{K}$, Fig. 9 shows the dependence of the minimum coherence in the steady-state oscillation on the coupling strength. Here the minimum steady-state coherence corresponds to the bottom of the troughs in the coherence after the system

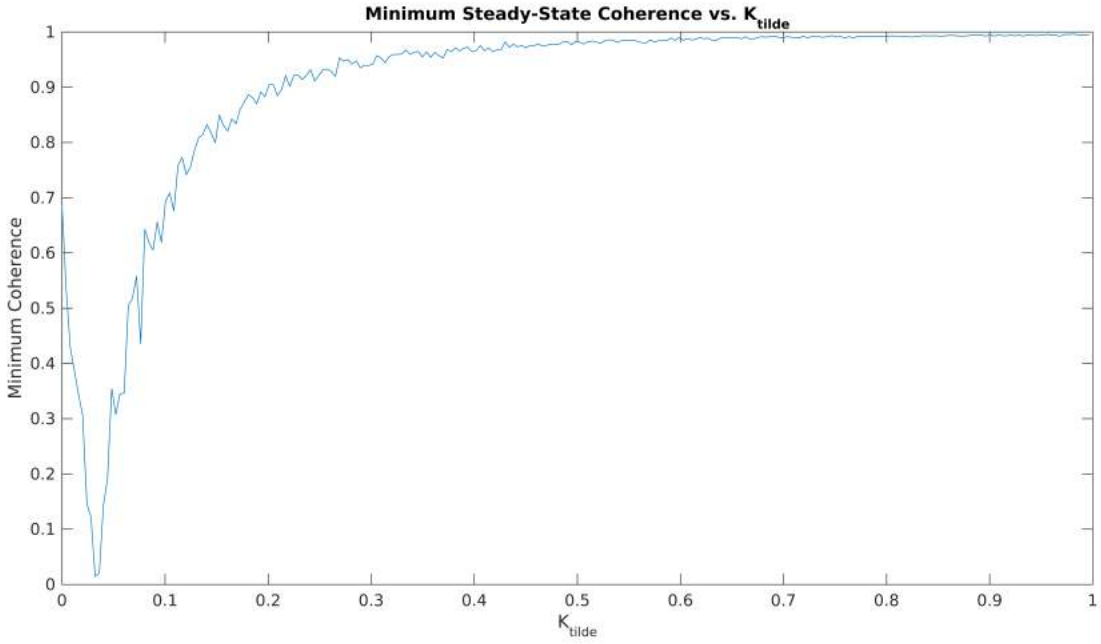

Figure 9: Numerical Simulation of minimum measured steady state coherence versus new coupling strength $\tilde{K}$. We see that the minimum coherence approaches 1 exponentially as $\tilde{K}$ increases. For $\tilde{K} = 0$, the phases spread and the coherence becomes noisy, however the fact that most of the oscillator time is spent in the quiescent state causes the coherence to be artificially high. The minimum coherence was obtained by taking the minimum value during the second half of the simulation lasting 10 seconds, using a time step of a $\frac{1}{10^{th}}$ milisecond, a b-value of .99, and a standard deviation of .05 ($\Omega = 8\pi$) over 100 oscillators.

has reached steady state. For example, the minimum for the oscillation in Fig. 8 would be just below 0.2.

Figure 9 suggests we can make qualitative predictions about the behavior of the periodic oscillations as a function of our new coupling strength. Given that the stability depends on λ, we can define a critical coupling in which $\lambda = 0$. Namely,

$$K_c = \frac{\Omega b}{r}$$
$$\Rightarrow \tilde{K_c} = \frac{1}{r}.$$

For $\tilde{K} > \tilde{K_c}$, the phase-locked state should always be stable. This in turn implies that the minimum coherence should be one because the system is perfectly synchronized. If the *minimum* coherence is one, then certainly r is one for the entire period.

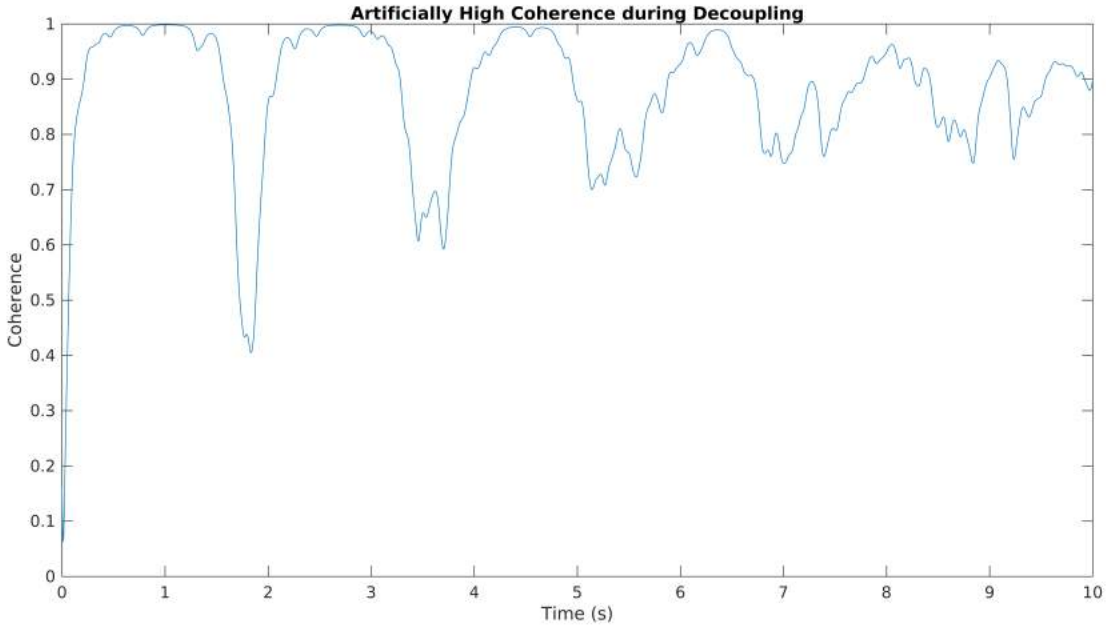

Figure 10: Artificially High Coherence for $\tilde{K} = 0$: All other conditions were identical to Fig. 9. As such, the left side of Fig. 9. is not a true synchronized state exhibiting periodic stability.

Therefore, the critical coupling in which the periodic stability disappears must occur at $\tilde{K_c} = \frac{1}{r}$, or $\tilde{K_c} = 1$. This circular nature of this argument may at first appear to invalidate the conclusions made. However, the relationship between $\tilde{K_c}$ and r is wholly self-consistent, and the assertions made are directly supported by the numerical experiments of Fig. 9. Indeed this approach is modeled after Kuramoto's pioneering work in the field [19]. Note that for 0 coupling, the phases spread freely. Since they spend most of their time in the quiescent state (i.e $\sin\phi = -1$), the coherence is artificially inflated. Therefore when functionally approximating the minimum coherence drop vs coupling, an offset is required.

As we can see, the drop in the coherence of the system can be explained using the periodic stability theory we have developed, and simulations are consistent with this theory. While we have developed a rudimentary understanding of the behavior of this system, there are numerous questions we can still ask. These questions are detailed in the further research section.

3 Experimental Observations of Periodic Stability

The primary result of the previous section states that the stability of the synchronized state of pulsing oscillations deteriorates in the pulsing regime of oscillator phase. The stability then re-materializes symmetrically during the quiescent portions of phase. This behavior implies that the phases will spread from one another during pulses and approach each other during quiescent states; the coherence of the system will oscillate. Our results thus far have deep implications for the behavior of a population of oscillators whose phase does not advance uniformly. When we examine the applications of the Kuramoto model, this indeed is the case for a large number of systems. In this section, the theoretical prediction of oscillating coherence will be tested and observed in both a numerical simulation of a large number of coupled neurons, and an experimental system of coupled Wien-Bridge oscillators.

The main results of the model are probed using numerical calculations based on the simulated phase of each oscillator in the model. Therefore, to probe the applicability of our results to this system, we need to somehow extract the phase from the voltage traces such as those given in Fig. 14.

An incredibly useful feature of our model is that the sine of the phase can be interpreted as the raw voltage output from the oscillator. That is, the pulses in Fig. 5 are directly representative of the pulses in the earlier neural voltage traces that were simulated. We can tune the amplitude of the sinusoidal output to match the maximum voltage of the system being modeled. With this in mind, the voltage traces produced by the experiments can likewise be interpreted as the output of sinusoids. Therefore our model assumes:

$$Observed\ Voltage = V_{max} \sin(\phi),$$

where ϕ is the phase of the oscillator being modeled. However, it is not always the case that V_{max} is a constant value. For the Wien-Bridge oscillators, the amplitude also varies over time. So that our problem can now be stated as: Given the output voltage, how can we calculate the phase of the oscillator if

$$Observed\ Voltage = V_{max}(t)\ \sin\phi(t)\ ? \tag{26}$$

The solution to this problem is nontrivial. In fact, we must use ideas developed from complex analysis to solve this problem. The tool we shall use here is the Hilbert transform. For the sake of staying on topic, the Hilbert transform will only be summarized and not explicitly derived.

3.1 The Hilbert Transform: How to extract phase from a Voltage Signal

The original motivation for developing the Hilbert transform stems from the following problem: If we have a real-valued function f: $\mathbb{R} \to \mathbb{R}$, does there exist an imaginary component g such that $h = f + ig$ can be analytically extended into the complex domain? [7]. That is, how can we project f onto the complex plain without changing its real component, f? An example relevant to our discussion is if $f = cos(x)$. The function satisfying this condition is $g = sin(x)$. Here $h = e^{ix}$ is the new complex function created from which we can easily get both f and g by taking the real and imaginary parts of h, respectively. In this example, f is a real function, and g is an imaginary function, and by combining the two to form the complex function, we can extend f into the complex domain without altering its behavior. Because of this, g is considered the *Hilbert Transform* of f. Allowing f to be a generic function, the Hilbert transform can be calculated as a convolution given by:

$$g(x) = \frac{1}{\pi} \int_{-\infty}^{\infty} f(u) \frac{1}{x-u} du \tag{27}$$

Hilbert transformers (circuits that output the Hilbert transform of a given input) have found useful application in cochlear implants, where each channel represents a frequency band of an acoustic signal. Receiving an acoustic signal given by $A(t)\ \cos\phi(t)$, an implant uses a Hilbert transformer to parse the amplitude and phase. [7] This is because every sinusoidal harmonic component of the input signal S_I is transformed, producing a transformed signal S_T. Essentially every harmonic component is shifted by 90 degrees by the transform. Cochlear implants connect to auditory nerves in the brain which are otherwise damaged and artificially produce parsed amplitude information. This amplitude information allows for some forms of auditory recognition in certain cases of the hearing-disabled. The transform of a signal S_T is related to the input signal, S_I, by:

$$S_T(t) = \frac{1}{\pi} \int_{-\infty}^{\infty} S_I(\tau) \frac{1}{t-\tau} d\tau \tag{28}$$

Note that for $S_I = \cos(\omega t)$, the transformed signal, $S_T = \sin(\omega t)$. Given the two signals, the original and its transform, the amplitude can be parsed as

$$A(t) \approx \sqrt{S_I^2 + S_T^2},$$

and the phase as:

$$\phi = \widetilde{tan^{-1}} \frac{S_T}{S_I}, \tag{29}$$

where S_T is given by the Hilbert transform of S_I. Note the tilde, which signifies that this is the 4-quadrant inverse tangent, which accepts arguments ranging from $-\pi$ to π. This is in contrast to the two-quadrant inverse tangent which only accepts arguments from -$\frac{\pi}{2}$ to $\frac{\pi}{2}$ We have given a purposefully brief glimpse into the Hilbert transform. For a more in-depth discussion and derivation, see [7]. As a final note, the Hilbert transform pairs S_I and S_T are one-to-one, meaning that there is only one Hilbert transform for a given signal. This means that S_T is unique to a given S_I, and therefore is not contrived to produce certain results.

Because our voltage signals are assumed to contain sinusoidal components with a varying amplitude, we thus have a method for extracting the phase from a periodic voltage signal as provided by the Hilbert transform. In previous work, the phase was artificially calculated from experimental data by measuring fundamental frequency of zero-crossing, and fitting this to a constant-amplitude sinusoidal curve. [5]

3.2 Comparison to Numerical Simulations of Neurons

Much of the introduction was devoted to uncovering the pulsing behavior of a neuron by building a model from basic physiological considerations. This analysis is now leveraged in terms of a numerical experiment. The persistent sodium plus potassium model which we used is biophysically precise, and experimentally accurate. Therefore we can trust the validity of this model as well as we would a neurophysiological data obtained in-vivo from a neural cell. [8] Analyzing a voltage trace, we first extract the phase.

Indeed our model appears to simulate the phase progression with fair accuracy. Thus we can say with some confidence that we are adequately capturing the dynamics of this single neuron with our model. Extending to the case of 50 coupled neurons subject to noise.

The two preceding figures demonstrate remarkable agreement between our model and that of a network of coupled neurons. The computational simplicity of our model relative to this previous network allows us to more easily simulate large networks of neurons as a result, and will assist in modeling networks of neurons as spiking oscillators.

3.3 Comparison to Experimental Measurements of Electrical Wien-Bridge Oscillators

Recent work with electrical Wien-Bridge oscillators [10] has shown that they are capable of being described by the Kuramoto model. The importance of this work

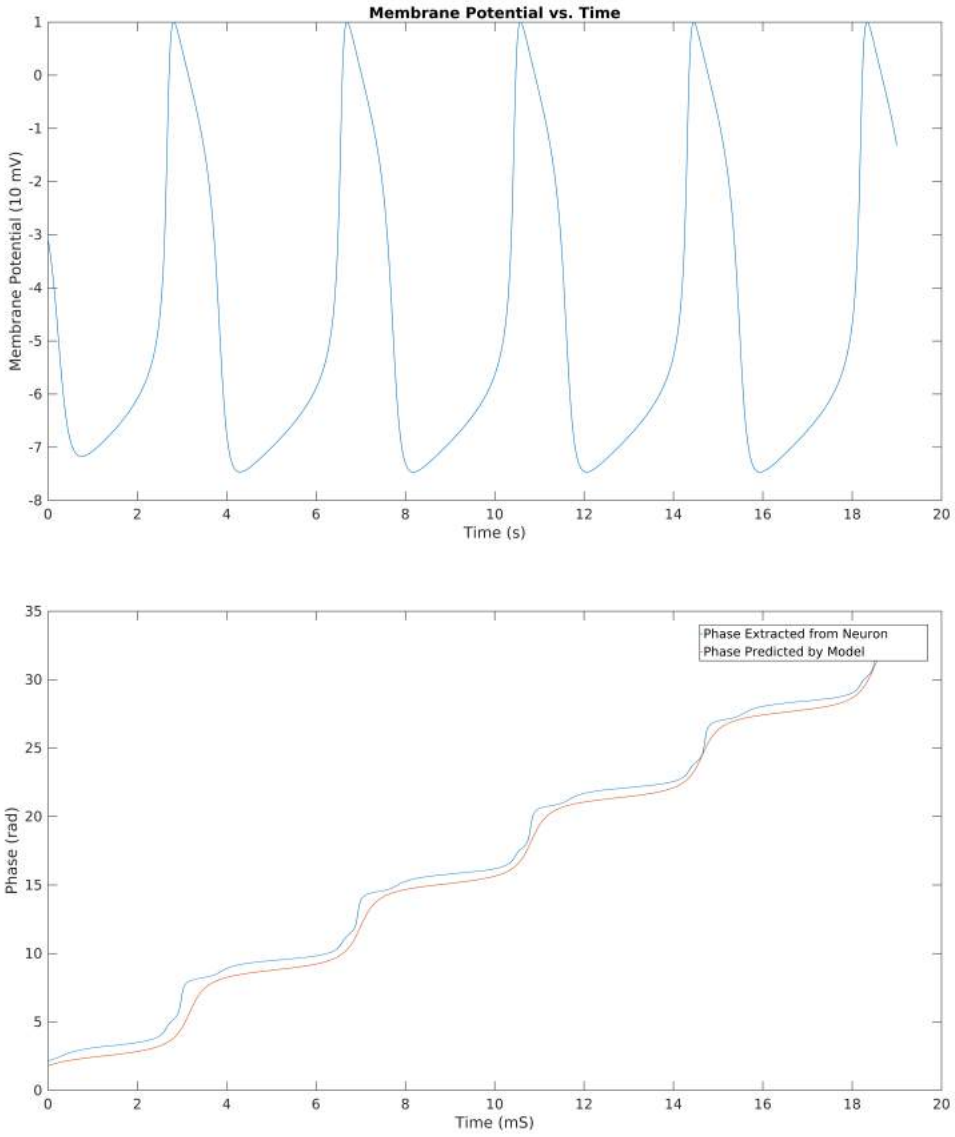

Figure 11: Top: The voltage trace of a single simulated neuron according to equation 7. Bottom: Extracted phase is calculated and the model data is fit to resemble this extracted phase. Although the wave forms are not identical, there is sufficient similarity in the dynamics of the two phases. Here, $b = .9$, and the initial condition of the phase model was set using the first data point of the experimental data.

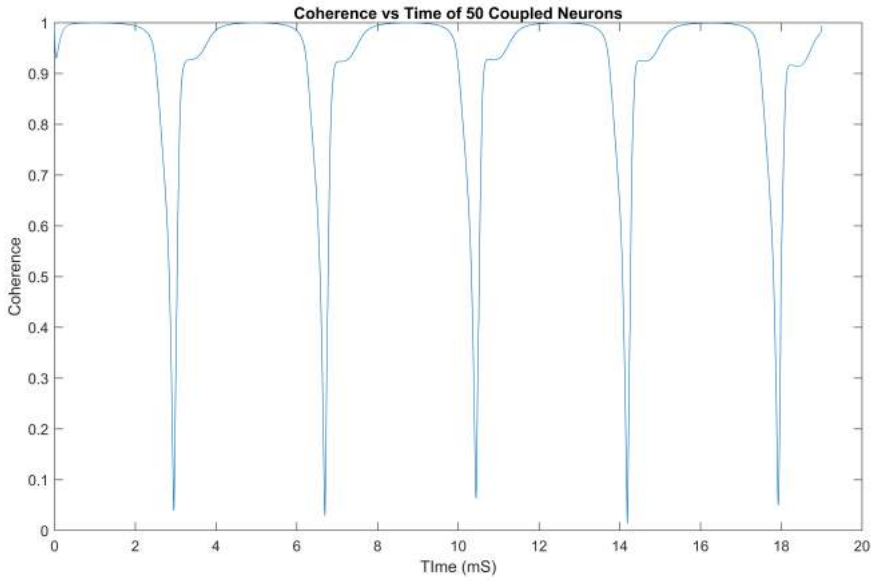

Figure 12: A simulation of 50 globally coupled neurons. They were also driven with Gaussian white noise with a SNR of 50 dB. A Kuramoto coupling scheme was used for the voltages of each oscillator and K = .2. Furthermore, the capacitances of each neuron followed a 10% standard deviation. Comparing this pseudo-experimental figure to Fig. 7 we see agreement in the essential oscillatory dynamics of the coherence.

is that the Kuramoto model emerges directly from the equations describing these oscillators, which themselves are simple applications of Kirchoff's laws. As such the behavior of this system is described accurately using the Kuramoto model.

The Wien-Bridge oscillators are in fact a type of relaxation oscillator. This means that a capacitor in the circuit is charged until it reaches a threshold potential before being rapidly discharged. As a result, the oscillator undergoes rapid periods of change as the threshold potential is reached, while otherwise exhibiting continuous charging. This oscillator thus exhibits pulse-like behavior, making it a prime candidate for applying our analysis. Furthermore, the results here should naturally extend to other relaxation oscillators: Chemical oscillations, the beating heart, turn signals; all are also considered relaxation oscillations. [6]

Figure 13: A circuit diagram of two coupled Wien-Bridge Oscillators. Adapted from English et al. [5]

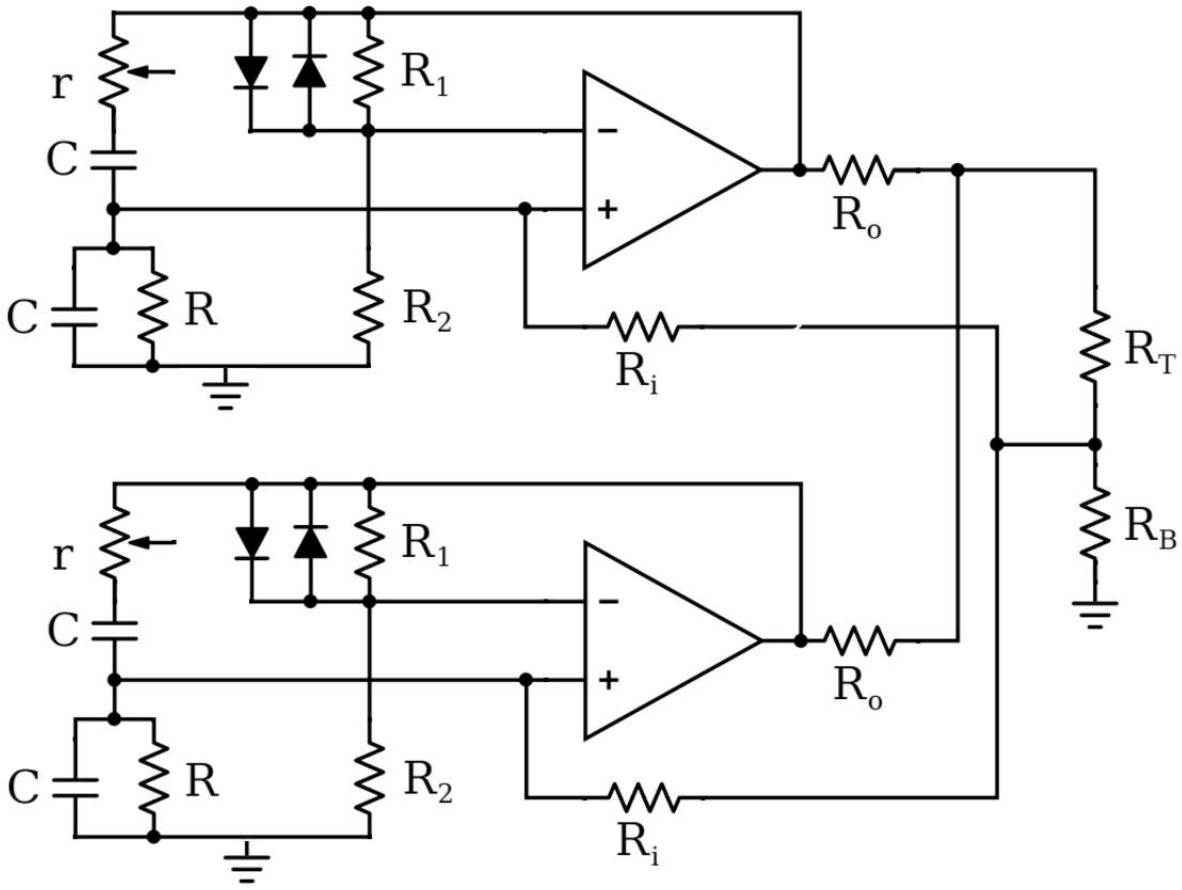

We see from Fig. 13 that the circuit of a single oscillator consists of an operational

amplifier (Op-Amp), along with an RC circuit joined together with an additional pair of diodes in opposite directions. These diodes introduce a voltage-dependent nonlinearity. Two such oscillators are coupled via resistors between the op-amps. Different coupling schemes can be used for arbitrary numbers of such oscillators. Namely, a ring topology was used whereby each oscillator is coupled to the next and previous neighbors, and the last oscillator is joined with the first. The specifics of the experimental setup are left to [5] [10]. Our primary purpose here is to analyze experimental data obtained from this system of oscillators and apply the predictions developed in the previous section.

Figure 14: An experimentally obtained voltage trace of a Wien-Brige oscillator in a coupled circuit of 20 such oscillators. The x-axis represents the sample number. The time is thus the sample number divided by the sampling frequency, $\frac{1}{10^{th}}$ milisecond

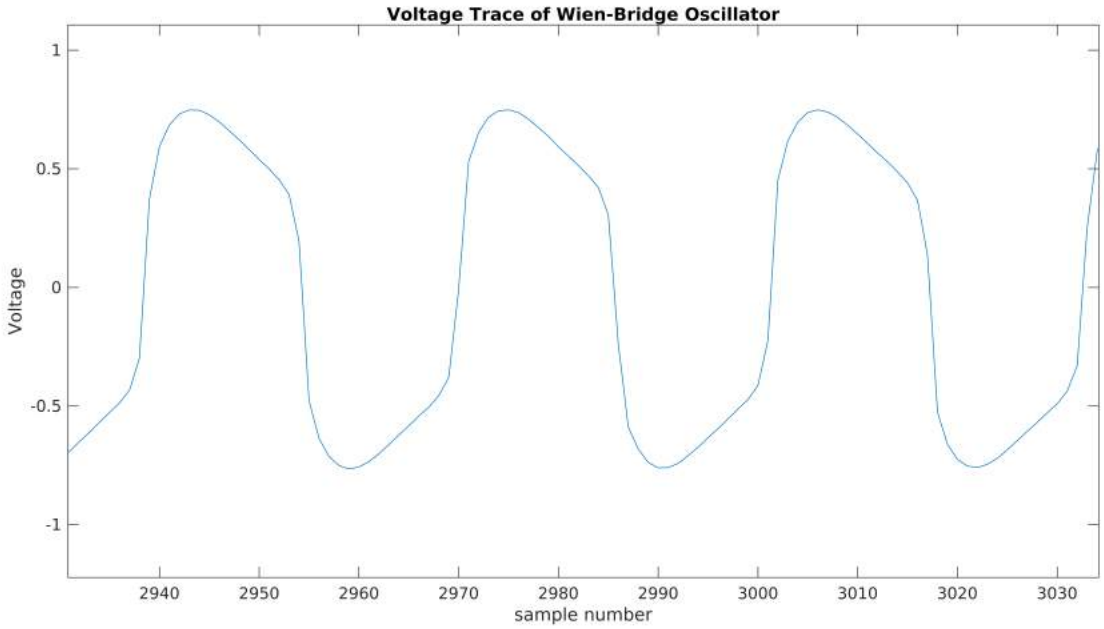

To that effect, Fig 14 presents an experimentally-measured voltage trace of a single Wien-Bridge oscillator that is coupled within a ring of 20 such oscillators. Although the signal appears sinusodal, it is clearly distorted to resemble that of a typical relaxation oscillator. The purpose of this figure is to provide evidence that the Wien-Bridge is, in fact, pulsing. In this case, the pulses are the sheer vertical leaps. In contrast to our model, however, there are two unique quiescent states that exist between pulses: a high and a low. This is relevant to our analysis further ahead.

Using Eq. (29), we calculate the phase of this oscillator, as shown in Fig. 15, as well as the amplitude given by the equation immediately preceding Eq. (29). With

both the phase and amplitude, we now can use the analytic tools developed in the previous section to characterize the system.

Now that we can satisfactorily extract the phase of the oscillator from the voltage trace, we can apply our analytic techniques. Namely, the coherence of the system.

We thus can clearly see the oscillations in the coherence of the system as predicted by our model. This offers sufficient evidence that the periodic stability is a tangible phenomenon. We also desire to observe the phase itself in time. Figure 17 displays an attempt to fit our model to the Wien-Bridge data presented. Although the waveform is qualitatively correct, the frequency of pulses during a single period is half of that of the Wien-Bridge phase. Therefore, we are motivated to modify our model to more accurately reflect the experimental data.

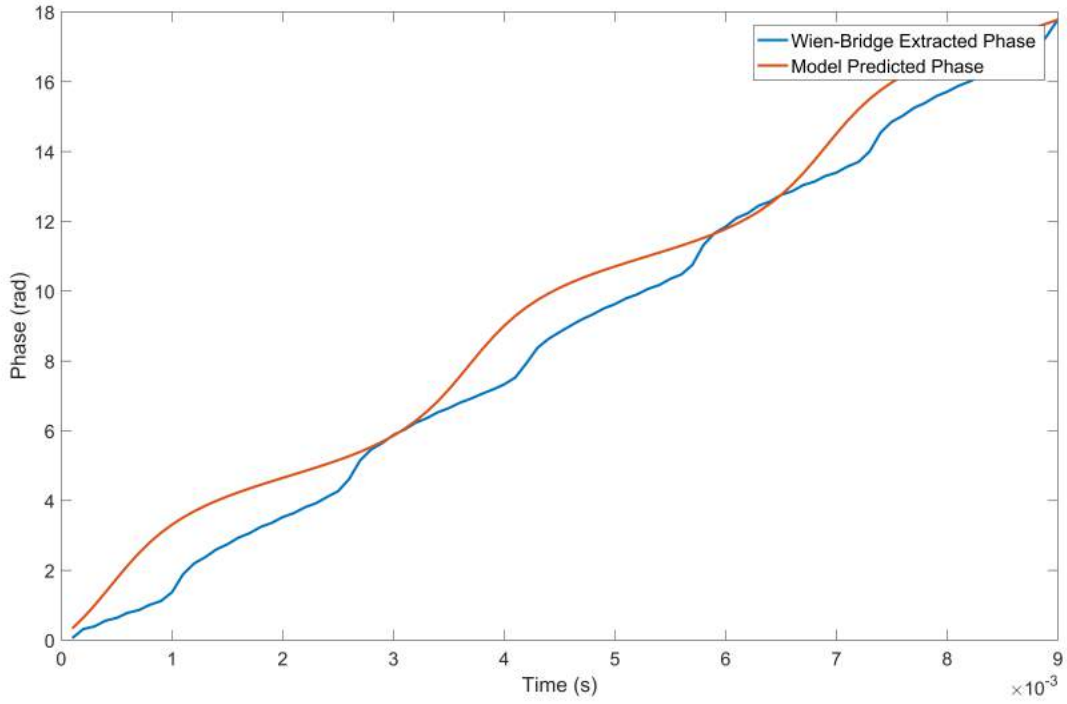

Figure 17: An attempt to fit our model to experimental Wien-Bridge data. Although our model captures the waveform correctly, the frequency of the pulses in a given period is half of that of the Wien-Bridge extracted phase. Therefore, to properly model this phase advancement, a modification to the model is needed.

During a single period of our current model, there is only one pulse that occurs. However the experimental system being modeled undergoes two pulses during a period, one from high to low, and the other from low to high. This is especially clear

Figure 15: Decomposition of experimental voltage data into phase and amplitude. Top: Cosine of phase as calculated using equation 29. Middle: Amplitude of phase as calculated using the equation immediately preceding 29. Bottom: The reconstructed voltage trace obtained by multiplying amplitude and phase, as described by equation 26. Compare this to Fig. 14. The two traces are, in fact, identical.

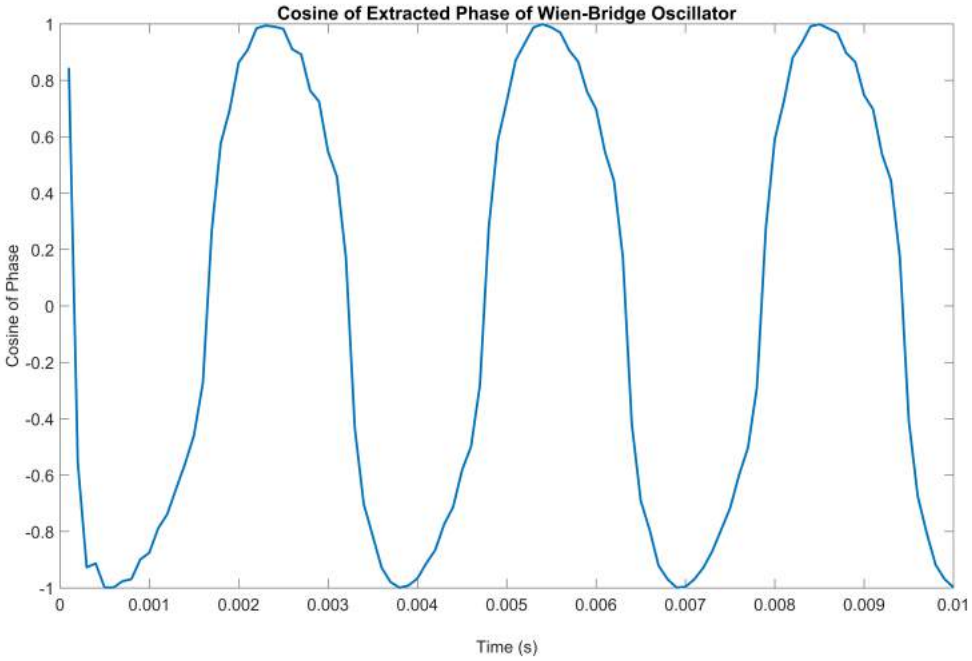

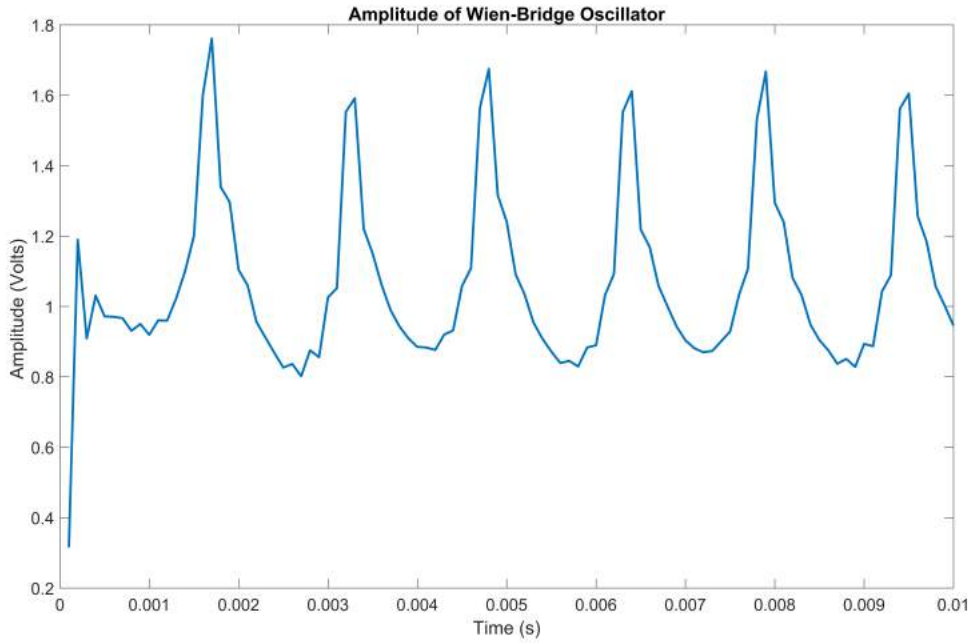

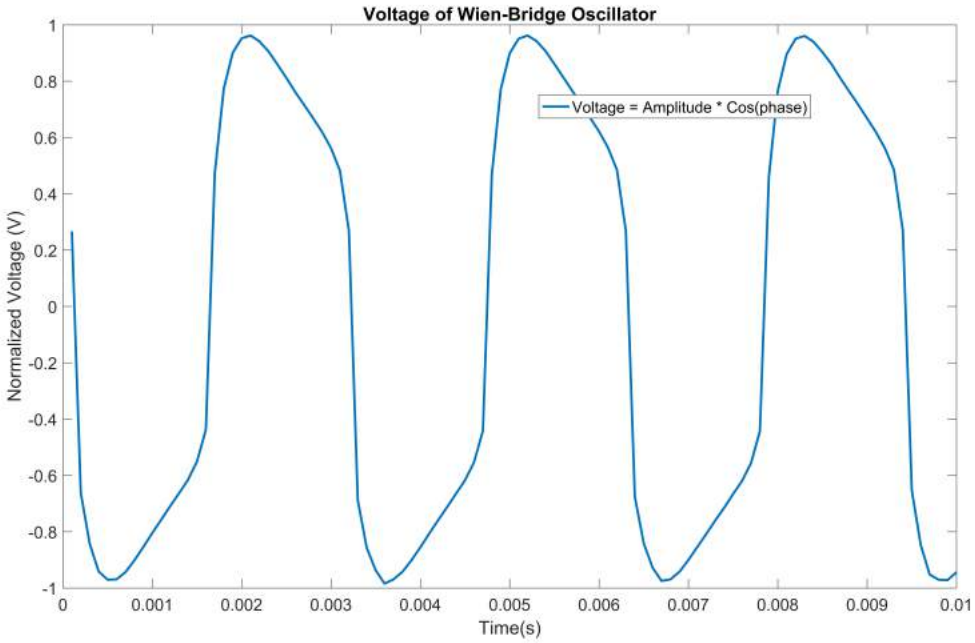

from Fig. 16, where the coherence indeed oscillates twice during period, a result consistent with both theory and experimental data. The source of pulsing in our model of a single oscillator Eq. (13) is the phase-dependency. The $\sin\phi$ term causes one pulse during a period as the argument undergoes one oscillation per period. These results lead us to an informed guess that two pulses would occur if the sine term underwent two oscillations per a single period of phase. Therefore we insert a two in the phase modulation term and observe the results. Thus our modified model is:

$$\dot{\phi} = \omega\big(1 + b\sin(2\phi)\big). \tag{30}$$

It is worth noting that although one may be tempted to simply use a change of variables to transform Eq. (30) into Eq. (13), the coupling term explicitly prevents this. That is, the coupled system of oscillators defined by Eq. (30) cannot be explicitly transformed into the system of coupled oscillators defined by Eq. (9).

When we now attempt to fit as in Fig. (17), we see much more clear agreement. To avoid redoing much of the analysis from section 2, we numerically simulate the phase of this altered oscillator and compare to the extracted phase of the Wien-Bridge Oscillator.

Figure 18 shows that this modification produces a significantly more accurate waveform for the Wien-Bridge oscillator. Thus our model is able to capture a significant portion of the dynamics of the oscillator using a single first-order differential

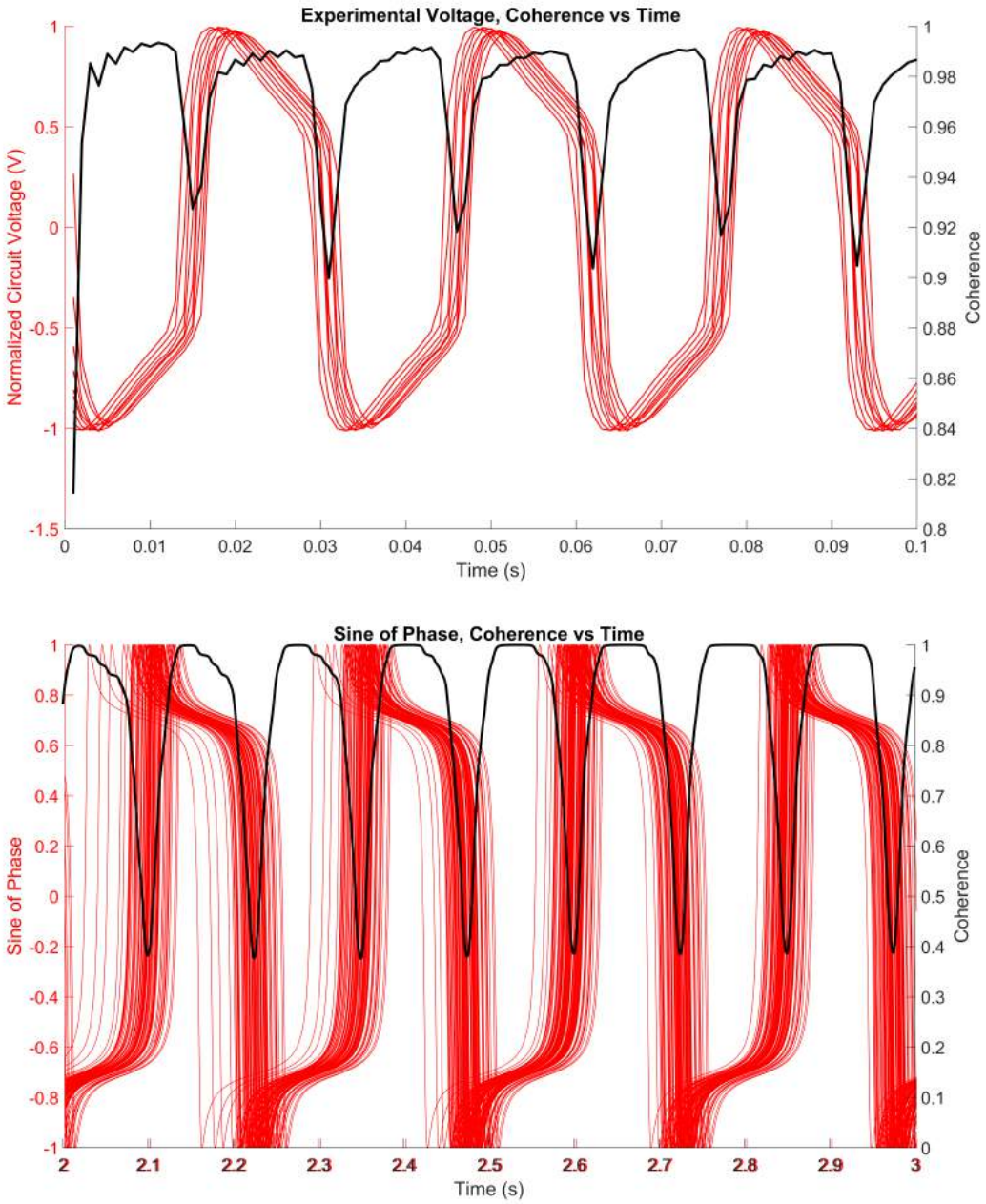

Figure 16: Top: Coherence vs time of 20 Coupled Wien-Bridge Oscillators with phase extracted using Hilbert Transform. Bottom: Coherence Oscillations in a simulation of the relaxation-type modification to the model. (See Below)The identical color of each voltage trace allows the clear depiction of the density increasing during the slow phases and the corresponding decrease during the vertical pulsing phases. This density corresponds to the coherence of the traces. Notably, the minimum coherence is constant in the simulation but varying in the experiment. The reason for this is that the two pulses per period are identical in the simulation (i.e the modulation is symmetric), whereas this is not necessarily the case in the experimental system. For the simulation $K = 1$, $\sigma = .05\Omega$, and $N = 100$.

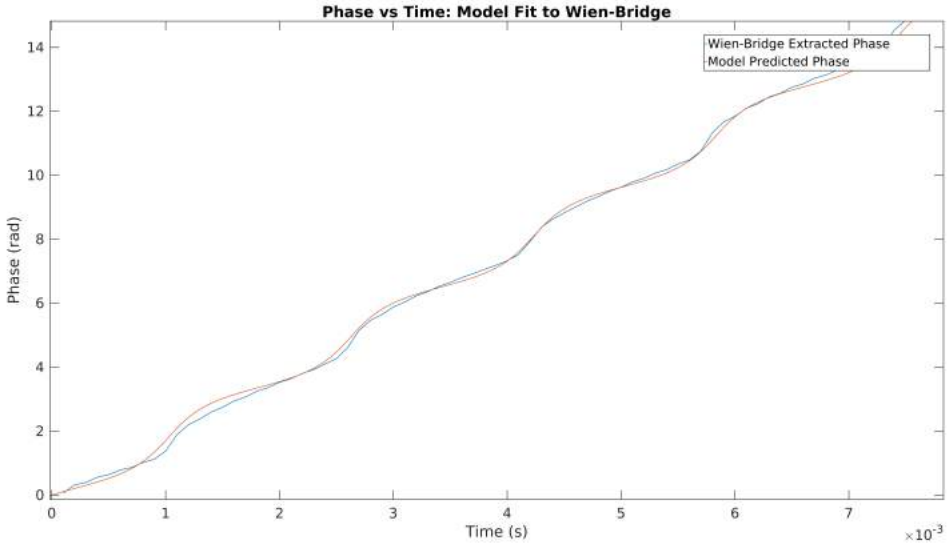

Figure 18: A fit of the modified model 30 to the extracted Wien-Bridge Phase. The fit is much more agreeable with this modification than the original model.

equation as opposed to a set of coupled second-order equations otherwise used to simulate these oscillators. [10] The Wien-Bridge is a particular type of relaxation oscillator. Since our model captures the dynamics of this oscillator, we argue that the essential dynamics of all relaxation oscillators are also captured by this modified model. The evidence offered in support of this assertion is given in Fig. 19. We see that the behavior of the modified model greatly resembles that of a van der Pol oscillator, which is an archetypal relaxation oscillator.

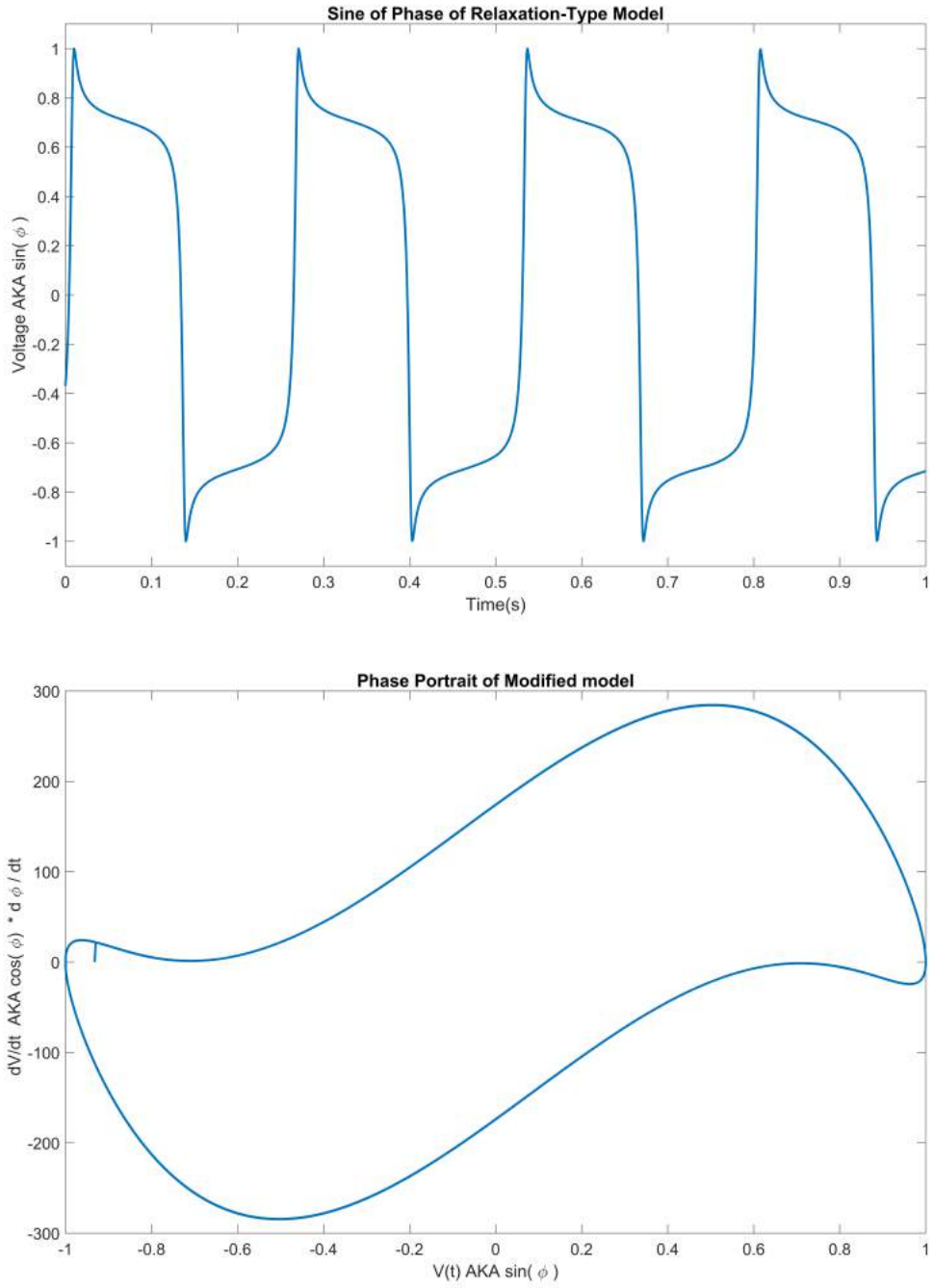

Figure 19: Top: The sine of the phase of the modified model simulated according to equation 30. Bottom: The calculated limit cycle obtained by numerically calculating the derivative of the sine of phase. Both of these figures share characteristics distinctive of relaxation oscillators. In particular, the limit cycle strongly resembles the deformations of a van der Pol oscillator. [6]

In this section we have presented evidence in two distinct experimental systems

that appreciably justifies the validity of our model. The oscillation in the coherence, as well as the nonlinearity of phase, are both novel predictions made by our model that are clearly visible in both experimental systems. The question that arises now is how do these new dynamics result in advantages over predictions made by the classical Kuramoto model? The exciting answers are detailed in the next section.

4 Explorations of Populations of Pulsing Oscillators

To this point we have devoted great effort in developing a model which more faithfully reflects the nature of a wide variety of systems. The implicit assumption made during this process was that the more nuanced picture of dynamics will yield novel and more useful predictions when we examine populations of pulsing oscillator. In this section, we will vindicate the previous work by studying the behavior of an ensemble of coupled oscillators and compare these results to the systems which they model.

4.1 Spiral Waves in a locally coupled lattice.

The Kuramoto model has been used to study populations of cortical neurons, and examine how certain neural oscillations develop. [13] Specifically, the Kuramoto model has been modified to include only local coupling via a spacial kernel. That is the coupling is enveloped by a function that is distance-dependent. Specifically, the function is the step function that is 1 if two oscillators are adjacent and 0 otherwise. In this way, a particular oscillator/neuron will explicitly alter only the phase of its adjacent neighbors. Although more complex coupling kernels such as the 4^{th} derivative spacial Gaussian [13] have been used, for computational simplicity, and as a first step we used adjacent coupling. This means that an oscillator only interacts directly with the 3x3 lattice where this oscillator is center. Explicitly,

$$\dot{\phi}_i = \omega_i(1 + b\sin\phi_i) + \frac{\tilde{K}}{8} \sum_{j=1}^{8\ local\ neurons} sin(\phi_j - \phi_i). \tag{31}$$

We thus use Kuramoto's coupling function but modify it to only cover the adjacent oscillators in the lattice.

Figure 20 displays the simulated lattice for the classic case where b = 0 (i.e a linear phase progression), and the novel case where b = .99. These dynamics only occur for appreciably high $\tilde{K}$. We see that the nonlinearity introduced by high b brings about significant new wave dynamics that self-organize within the system. Such oscillations

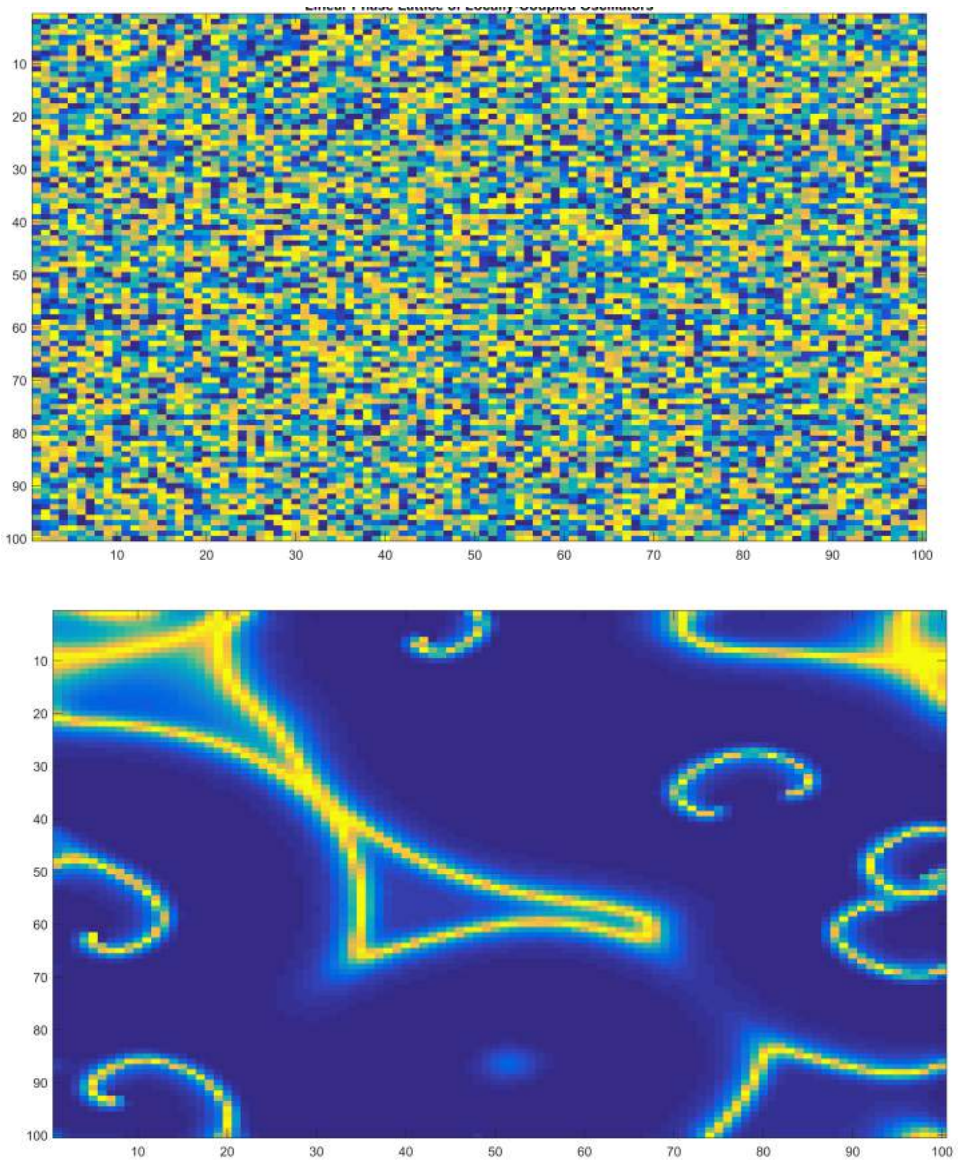

Figure 20: Simulations of locally coupled lattices using a linear-phase (top) and novel nonlinear (bottom) oscillator paradigm. The linear case induces near-global synchrony whereas the nonlinear novel case produces spiral patterns as observed in real chemical and biological systems. In a locally coupled lattice, each oscillator is connected to only the immediate adjacent oscillators, including diagonally via the sinusoidal phase difference. Periodic boundary conditions were imposed in both directions, and both simulations used a timestep of a tenth-milisecond, with $\tilde{K} = .99$, and a Gaussian distribution of frequencies with a mean of 3π and a standard deviation of $.02\Omega$.

are an observed phenomenon in neural systems. [14] Thus our model offers useful explanations and predictions of observed neural phenomena.

Shinomoto and Kuramoto showed that a lattice of such pulsing active rotators could not exhibit fully synchronous dynamics for sufficiently high values of b; namely that noise easily destroys the result with a sensitivity controlled by b. [21] Furthermore, they also showed that the vorticity of an arbitrary loop decreased logarithmically with b. Given the results of Fig. 9, however, we expect a phase transition to occur as a function of coupling strength. Even for a highly nonlinear system (b=.99), the spirals only appear for sufficiently high coupling ($\tilde{K}$ roughly greater than .2) . As such a point of further research includes investigating the transition between the uncoupled, sponge-like lattice and the tightly bound spiral-producing lattice.

The waveforms predicted by this model strongly resemble the spiral wave structures produced by the Belousov−Zhabotinsky reaction. [20] As such, the active rotator model offers useful predictions that have been observed in both chemical and biological systems.

5 Conclusions and Further Research

The fundamental purpose of work in this field is to analyze systems of coupled oscillators and their behavior. To this effect, the Kuramoto model has been leveraged to describe how various systems synchronize, as well as under what conditions. This model has been used to great effect to explore a wide variety of systems found universally in nature as well as in man-made constructs. However, this model is limited in its abstraction.

Our modification allowed us to introduce a phase non-linearity, which we now consider a defining feature of pulsing oscillations. This non-linearity via the spacial modulation of frequency introduced a novel dynamical behavior that more accurately reflects a large number of systems typically modeled by the Kuramoto equation.

We have explored this new model and discovered novel dynamics such as periodic stability and wave self-organization. As such this model may yield new results when applied to systems typically analyzed using linear phase. We have thus devoted significant time and effort to exploring this novel model.

However, there are a large number of unanswered questions about this system. Can we derive an analytic expression for the mean phase of an ensemble of pulsing oscillators? Our best guess was an approximation that yielded useful analytic results, but we do not have definitive proof that the guess was correct beyond a moderately convincing numerical simulation. How does the synchrony of the system depend

on the coupling strength? Once again we have probed this idea using numerical simulations, but we are at a formal analytic loss to fully explain why the system behaves in this way. Another area of further research might seek to analyze the modified model we used to reproduce the relaxation oscillator. This model therefore demonstrates flexibility in how it models pulsing systems and further research would explore the extent and usefulness of this flexibility. Finally, the simulations involving populations of oscillators offers a large variety of research paths that may be taken. Different coupling schemes such as the more sophisticated cortical-based kernel could be implemented. That is, the coupling envelope could be implemented in a more physically plausible manner to represent different brain regions an densities. Lattices may be extended to cubes and the volumetric behavior may be explored. Complex network topologies could be implemented, and finally the relaxation-type oscillator could also be implemented in different topological structures.

Overall, our system provides a unique and more accurate description of the behavior of pulsing systems without any additional computational complexity. As such, this model can be used to further push the boundaries of nonlinear science in new productive directions.

A Appendix

A.1 Matlab Code for 2 Coupled Neurons

Contents

Setup and Header

```
%Christopher Fritz
%I_Na,p + I_K model (Reduced);
%2 Neurons Are Gap-Junction Coupled
%The first Neuron is driven by current I,
%The second is undriving, except for coupling to other neuron
% 10/10/2016
clear;
clc;
close all;
```

Diffeqs Describing the System:

```
% C(dV/dt) = I - g_L * (V - E_L) - g_Na * m_inf(V) * (V - E_Na)
         %   - g_K * n(V) *(V - E_K)

% dn/dt = (n_inf(V) - n) / tau_n (V)
% assume m = m_inf
%
%
% V and n are the dynamical variables we wish to graph/analyze:

%-------------------------------------------------------------------------

% Steady State Activation Curve is approximated by the Boltzmann Function:
% m_inf(V) = [  1 + exp{ (V_1/2 - V) / k }  ] ^-1 ;
        % m_inf(V_1/2) = .5
        % k = slope factor: smaller k--> steeper curve

% The voltage sensitive time-constant is modelled by the Gaussian Function:
% tau(V) = C_base + C_amp * exp{ -(_Vmax - V)^2  / sigma^2 }
        % C_base = lowest value function reaches after Gaussian Decay
        % C_amp  = Height of Gaussian at Max from C_base
        % V_max  = Value at which Gaussian is Maximum

%-------------------------------------------------------------------------
```

Physical Parameters (as defined in Izhikevich fig. 4.1, pg. 90):

```
C      = 1;     %Mean Capacitance                    (micro? F)
I      = 40;    %Mean Total Current Flow           (mA / cm^2)
E_L    = -80;   %Leak Current Equilibrium Potential  (mV)
E_Na   = 60;    %Sodium Equilibrium Potential        (mV)
E_K    = -90;   %Potassium Equilibrium Potential     (mV)
g_L    = 8;     %Leak Current Conductance            (mS/cm^2)
```

```
g_Na   = 20;    %Sodium Current Conductance          (ms(cm^2)
g_K    = 10;    %Potassium Current Conductance       (mS/cm^2)
m_half = -20;   %Half-Voltage of m curve             (mV)
k_m    = 15;    %Slope factor of m curve             (mV)
n_half = -25;   %Half-Voltage of n curve             (mV)
k_n    = 5;     %Slope factor of n curve             (mV)
tau    = 1;     %Voltage Sensitive time-constant     (sec)
K      = 1;    %Coupling Constant (Conductance)     (mS/cm^2)
```

Simulation Parameters

```
N      = 2;      %Number of Simulated Neurons
dt     = .001;   %Time Step Interval             (s)
V_0    = 30;     %Initial Voltage                (mV)
n_0    = .50;    %Initial Activation of K+ gates (probability)
T      = .02;
```

Initialization

```
Is       = normrnd(I,0*I,N,1);       %Gaussian distribution of current
Cs       = normrnd(C,.0*C,N,1);      %Gaussian distribution of capacitance
V_t      = zeros(N,T/dt);            %Membrane Potential
n_t      = zeros(N,T/dt);            %K+ activation-gate proability
m_inf    = zeros(N,T/dt);            %Steady-State Activation of Sodium
n_inf    = zeros(N,T/dt);            %Steady-State Activation of Potassium
V_t(:,1) = -normrnd(V_0,0*V_0,N,1);  %Random initial voltages
n_t(:,1) = n_0;                      %Initial K+ Conditions
count    = 1;
ts       = zeros(1,T/dt);

%%Run The Simulation

%For Each Iteration:
for i = 1:dt:T/dt
    for j = 1:N
   %Calculate Steady State Acvitation Functions
   m_inf(j,count) = (  1 + exp( ( m_half - V_t(j,count) ) / k_m )  ).^-1;


   n_inf(j,count) = (  1 + exp( ( n_half - V_t(j,count) ) / k_n )  ).^-1;



   %Calculate and Record Next Voltage and K+ values, insert noise
   V_t(j,count+1)  = awgn(V_t(j,count) +  (   Is(j,1) - g_L * (V_t(j,count) - E_L)...
            - g_Na * m_inf(j,count) * (V_t(j,count) - E_Na) ...
            - g_K * n_t(j,count) *(V_t(j,count) - E_K) + (K/N)*sums(V_t(:,count)) )*(dt/Cs(j,1)),30);

   n_t(j,count+1) = (n_t(j,count) + ( (n_inf(1,count) - n_t(1,count)) / tau ) * dt) ;

    end
    %update time
    ts(1,count+1) = ts(1,count) + dt;
    count = count +1;
end



%%Plot Phase Portrait and Voltage Trace
```

```
figure
plot(ts,V_t)
title('Membrane Potential vs Time')
xlabel('Time (s)');
ylabel('Membrane Potential (mV)');
```

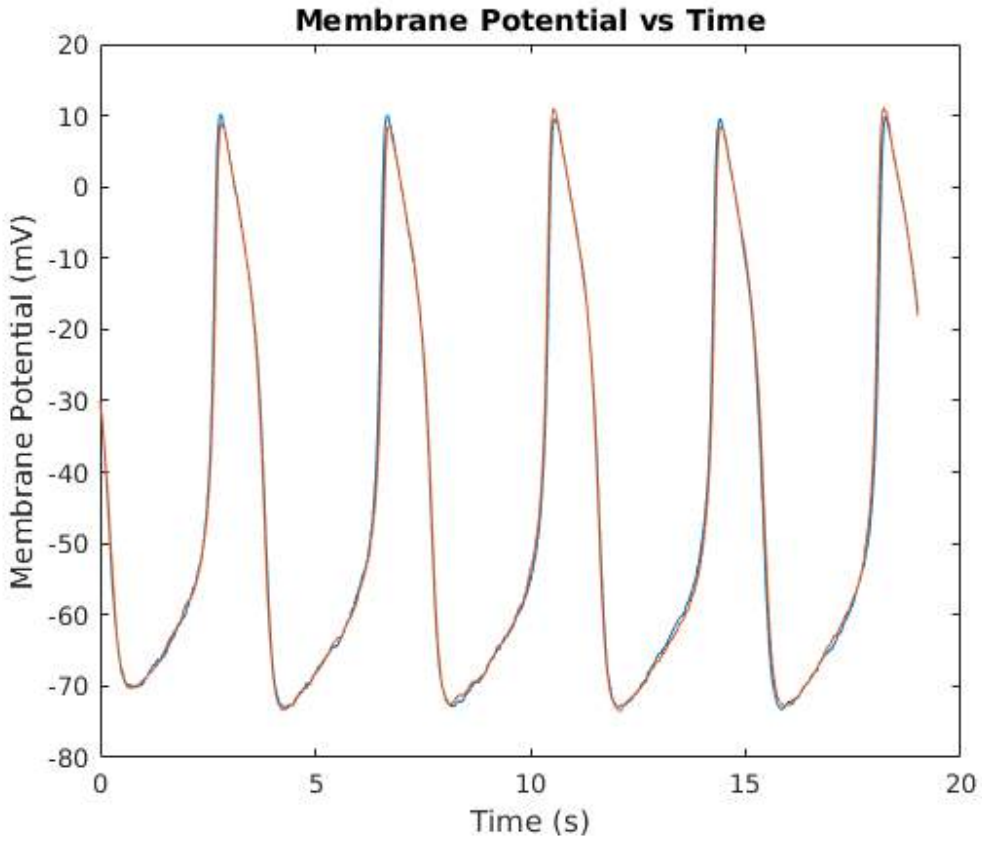

Published with MA TLAB® R2016a

References

[1] Figure courtesy of Dr. C. George Boeree; http://webspace.ship.edu/cgboer/theneuron.html

[2] L.Q. English, K. Skowronski, P.G. Kevrekidis, Saidou Abdoulkary, C.B. Fritz, David Mertens, "Direct observation of the chimera state in a ring of coupled electronic self-oscillators". Under Review

[3] Abrams, Daniel M., and Steven H. Strogatz. "Chimera States for Coupled Oscillators." Physical Review Letters 93.17 (2004): Web.

[4] Dayan, Peter, and L. F. Abbott. "Neural Encoding I: Firing Rates and Spike Statistics." Theoretical Neuroscience: Computational and Mathematical Modeling of Neural Systems. Cambridge, Mass.: MIT, 2001. 3-44. Print.

[5] English, L. Q., Zhuwei Zeng, and David Mertens. "Experimental Study of Synchronization of Coupled Electrical Self-oscillators and Comparison to the Sakaguchi-Kuramoto Model." Physical Review E 92.5 (2015): Web.

[6] Jean-Marc Ginoux, Christophe Letellier. Van der Pol and the history of relaxation oscillations: toward the emergence of a concept. Chaos, 2012, 22, pp.023120.

[7] Yi-Wen Liu (2012). Hilbert Transform and Applications, Fourier Transform Applications, Dr Salih Salih (Ed.), InTech, DOI: 10.5772/37727. Available from: http://www.intechopen.com/books/fourier-transform-applications/hilbert-transform-and-applications

[8] Izhikevich, Eugene M. *Dynamical Systems in Neuroscience: The Geometry of Excitability and Bursting.* Cambridge, MA: MIT, 2007. Print.

[9] Shinomoto, S., and Y. Kuramoto. "Phase Transitions in Active Rotator Systems." Progress of Theoretical Physics 75.5 (1986): 1105-110. Web.

[10] L. Q. English, David Mertens, Saidou Abdoulkary, C. B. Fritz, K. Skowronski, and P. G. Kevrekidis, "The emergence and analysis of Kuramoto-Sakaguchi-like models as an effective description for the dynamics of coupled Wien-bridge oscillators". To appear in Physical Review E.

[11] Staff, By Mayo Clinic. "Depression (major Depressive Disorder)." Selective Serotonin Reuptake Inhibitors (SSRIs). Mayo Foundation for Medical Education and Research, n.d. Web. 27 Oct. 2016.

[12] Novikov, A.V, Benderskaya E. N., Oscillatory neural networks based on the Kuramoto model for cluster analysis, Pattern Recognition and Image Analysis, 2014, Volume 24, Number 3, Page 365

[13] Breakspear, Michael, Stewart Heitmann, and Andreas Daffertshofer. "Generative Models of Cortical Oscillations: Neurobiological Implications of the Kuramoto Model." *Frontiers in Human Neuroscience Front. Hum. Neurosci.* 4 (2010): Web.

[14] Schnitzler, Alfons, and Jaochim Gross. "Normal and Pathological Oscillatory Communication in the Brain." Nat. Rev. Neurosci. 6.4 (2005): 285-96. Web.

[15] Purves, Dale. *Neuroscience.* Sunderland, MA: Sinauer, 2008. Print.

[16] Strogatz, Steven H. "From Kuramoto to Crawford: Exploring the Onset of Synchronization in Populations of Coupled Oscillators." Physica D: Nonlinear Phenomena 143.1-4 (2000): 1-20. Web.

[17] Strogatz, Steven H. *Nonlinear Dynamics and Chaos: With Applications to Physics, Biology, Chemistry, and Engineering.* Reading, MA: Addison-Wesley Pub., 1994. Print.

[18] Wolfram Alpha LLC. 2016. Wolfram—Alpha. https://www.wolframalpha.com/input/?i=integrate+(dx+%2F+(1%2Bbsinx)+) (access July 10, 2016).

[19] Kuramoto, Yoshiki. Chemical Oscillations, Waves, and Turbulence. Berlin: Springer-Verlag, 1984. Print.

[20] Zhang, D., L. Gyorgyi, and W. R. Peltier. "ChemInform Abstract: Deterministic Chaos in the Belousov-Zhabotinsky Reaction: Experiments and Simulations." ChemInform 26.1 (2010): n. pag. Web.

[21] Shinomoto, S., and Y. Kuramoto. "Cooperative Phenomena in Two-Dimensional Active Rotator Systems." Progress of Theoretical Physics 75.6 (1986): 1319-327. Web.